A review of heat transfer of CO_2 at supercritical pressure in the critical and pseudo-critical region

Lei Chai* and Savvas A Tassou

Centre for Sustainable Energy Use in Food Chain (CSEF), Institute of Energy Futures, Brunel University London, Uxbridge, Middlesex UB8 3PH, UK

Abstract This paper presents a comprehensive analysis of heat transfer characteristics and correlations for CO_2 at supercritical pressure in the critical and pseudo-critical region. Firstly, the thermophysical properties of CO_2 are discussed along with their influence on heat transfer characteristics. This is followed by a review of existing experimental and numerical studies on heat transfer and pressure drop for different channel geometries (smooth tubes, porous tubes, concentric annular passages, micro-fin tubes and helical coils), covering hydraulic diameters from 0.27 to 22.8 mm and bulk temperature from 0 to 120 ^oC and pressure from 74 to 150 bar, as well factors influencing heat transfer. The review of published works shows that the heat transfer characteristics are influenced by the geometry configuration and operating conditions, including channel shape and dimension, mass flux, heat flux, bulk temperature and pressure, flow direction, buoyancy, and heating or cooling conditions. Detailed comparisons and analysis of available heat transfer correlations for CO_2 at supercritical pressure are discussed and the review shows that there is lack of universal correlations able to accurately describe local heat transfer and pressure drop for different channel geometries and in particular for the pseudo-critical region. The paper identifies research gaps and proposes research and development needs to fill these gaps to ensure that reliable heat transfer and pressure drop correlations are developed to cover a wider range of operating conditions and applications.

Keywords heat transfer; pressure drop; carbon dioxide; supercritical pressure; critical and pseudo-critical region.

* Corresponding author. Tel.: +44 (0)1895 265834.

E-mail address: Lei.Chai@brunel.ac.uk (Lei Chai).

1. Introduction

Carbon dioxide (CO_2) is becoming an important commercial and industrial fluid due to its environmental credentials and its advantageous characteristics, such as being nontoxic and non-flammable and having low viscosity and a large refrigeration capacity. Due to growing environmental awareness and concerns, CO_2 is becoming increasingly popular as a natural refrigerant since it has a negligible impact on global warming [1, 2, 3]. Moreover, it is inexpensive and readily available, with demonstrated performance that is competitive when compared to those currently in use [4, 5]. The use CO_2 as a refrigerant has now become well established in commercial refrigeration applications globally [6], and high temperature heat pumps systems for domestic hot water heating in Japan [7]. CO_2 heat pump systems for both space and domestic hot water heating are also commercially available from a number of Japanese manufacturers and their adoption for space heating in commercial applications is increasing to displace gas boilers [8]. There is also increasing interest in the development of high temperature heat pumps, above 100 ^oC, for industrial applications [9].

Further, due to globally increasing demand for electrical power and the drive to displace the use of fossil fuels in power generation, the supercritical CO_2 Brayton cycle has recently been gaining a lot of attention for application to power generation and heat to power conversion systems, especially where heat-source temperatures are in the range of 400 to 900 °C [10]. Such applications include concentrated solar power plant, new generation of nuclear reactors and high temperature waste heat to power conversion [11, 12]. Advantages of supercritical CO_2 (sCO_2) power plant over conventional steam Rankine, gas turbine and organic Rankine cycle systems include higher efficiencies and smaller footprint which can lead to improved economics.

The heat exchangers are key components in CO_2 systems as they have a large influence on the overall efficiency of the system and cost [13]. As a result, significant attention has been placed on the investigation of CO_2 and its heat transfer and pressure drop characteristics in compact heat exchangers. Despite this, however, there is still significant uncertainty on the selection of the most appropriate correlations to use particularly close to the critical point. The aim of this review is thus to comprehensively summarize the available literature on heat transfer and pressure drop in systems employing CO_2 at supercritical pressure and flowing inside channels, including discussion of experimental and numerical investigations, and assessing heat transfer and pressure-drop correlations.

2. Thermophysical properties of CO_2 at supercritical pressure

Heat transfer in the critical and pseudo-critical region is significantly influenced by changes in thermophysical properties. This is particularly important for the creation of generalized correlations in non-dimensional form and, therefore, for the design of heat exchangers [14, 15]. The thermophysical properties of CO_2 at different temperatures and pressures, including the supercritical region, can be calculated using the National Institute of Standards and Technology (NIST) Standard Reference Database REFPROP V9.1 [16]. Fig. 1 shows the variation of the thermophysical properties of CO_2 with temperature, for pressures ranging from 80 to 200 bar. It can be seen that the properties change drastically with temperature in the critical and pseudo-critical regions: the density and dynamic viscosity abruptly decrease, while the specific heat undergoes a sharp increase within a very narrow temperature range; in addition, the thermal conductivity experiences a sharp side close to the pseudo-critical points. These changes become less pronounced with an increase in pressure.

These variations in the thermophysical properties close to the pseudo-critical points make the heat transfer performance of CO_2 different from other fluids, especially in the determination of the convective heat transfer coefficient and pressure drop [17, 18]. Good knowledge of the thermophysical properties is therefore very important for the calculation of heat transfer and pressure drop in the design of supercritical CO_2 heat exchangers – where the *ε-NTU* and LMTD methods usually require nearly constant specific heat and thermal conductivity over the design section. As a result, when measurements or thermal designs are made, careful attention should be paid to these values to assess whether they remain relatively constant or vary significantly [19].

3. Heat transfer characteristics of CO_2 at supercritical pressure

Many researchers have performed experimental and numerical investigations to determine the heat transfer characteristics of CO_2 at supercritical pressure for different channel geometries and dimensions, as well as different operation conditions.

3.1 Horizontal channels

A summary of studies on the thermohydraulic performance of CO_2 flowing inside horizontal channels is presented in Table 1 in chronological order. The table details the method used in the investigation, theoretical and/or experimental, the range of operating conditions (temperature and pressure, heat flux, flow rate, heating

or cooling) and details of the channel geometry. The factors influencing heat transfer performance investigated, are listed in Table 2. These include: mass flux, heat flux, bulk temperature, pressure, tube diameter and buoyancy.

The temperature of the CO_2 has a significant influence on the specific heat, and thus, on the heat transfer performance. The rapid increase in the specific heat near the pseudo-critical region (see Fig. 1c) causes a sharp rise in the heat transfer coefficient, which reaches a maximum very close to the pseudo-critical temperature, before decreasing sharply. The peak in the specific heat reduces as the pressure increases and happens at a high temperature. This then leads to a reduction in the heat transfer coefficient. The channel diameter and the mass flux mostly determine the Reynolds number of CO_2 flowing inside channels and can have a large influence on the local heat transfer coefficient. At a given pressure, increasing the CO_2 mass flux will usually lead to a higher heat transfer coefficient and a higher pressure drop. Fig. 2(a) shows the variation of heat transfer coefficient for cooling in horizontal tubes of 4.55 mm internal diameter and mass flux of 400 kg/(m^2 s) with bulk temperate, and pressure. It can be seen that for a pressure of 75 bar, increasing the bulk temperature causes a sharp rise in the heat transfer coefficient reaching a maximum of 17 kW/(m^2 K) before it begins to decrease with further increases in temperature. For higher pressures of 85 bar and 95 bar the peak heat transfer coefficient is lower, at the pseudo-critical point before it starts reducing slowly. Away from the pseudo-critical points the heat transfer coefficient is higher for the higher pressures at the same temperature. From Fig. 2b, it can be seen that increasing the mass flux for a constant pressure leads to an increase in the heat transfer coefficient along the temperature range and the peak value at the pseudo-critical point. These effects are mainly due to the influence of the thermophysical properties of the CO_2 close to the pseudo-critical point and the influence of the mass flux on the Reynolds Number of the CO_2 flow in the tube. These effects close to the pseudo-critical point are generally independent of the process, heating or cooling.

Fig. 3 shows the effect of heat flux on the heat transfer coefficient for horizontal flow in in semi-circular microchannels in heating and cooling modes adapted from Li et.al. [34]. It can be seen from Fig. 3a, that increasing the heat flux has a decreasing effect on the heat transfer coefficient in the heating mode. This is due to the reducing influence of the specific heat and thermal conductivity of CO_2 on heat transfer, across the wall of the channel, as the boundary layer of the flow reduces with increasing heat flux. Fig. 3b, shows that increasing the heat flux has negligible impact on the heat transfer coefficient at bulk temperatures below the pseudo-critical

temperature. At temperatures above the pseudo-critical temperature, increasing the heat flux tends to increase the heat transfer coefficient. The investigators [34], attributed this to the faster cooling effect at the higher heat flux (cooling), which reduces the film temperature of the flow in the pipe below the pseudo-critical temperature, thus increasing the influence of the specific heat and thermal conductivity of the CO_2 on heat transfer. Ehsan et.al. [47] investigated the heat transfer deterioration under heating mode and claimed that the influence of heat flux on the heat transfer coefficient was particularly important in heating mode and much different from the cooling mode. With increase of the ratio of the heat flux to the mass flux, the wall temperature increases to an earlier peak and causes the reduction of turbulent production in the near wall regime which deteriorates the heat transfer. After beyond the pseudocritical temperature, the sharp decrease of density results in distortion of shear stress and significant reduction of turbulent production. Therefore, the heat transfer coefficient experiences normal, improved and deteriorated process with increased heat flux. Jackson [48] pointed out that the heat transfer depends on the strength of the heating: low heat flux leads to enhancement while high heat flux results in deterioration. The heating strength determines the sharp variation of thermal properties and the flow acceleration due to the density reduction and thus the heat transfer process.

From Table 1, it can be seen that most of the literature relate to experimental investigations. Very few studies have been performed using simulation and analytical methods, due to the difficulty in capturing the effect of the extremely large variations in the thermophysical properties of CO_2 close to the critical or pseudo-critical point. Pitla et al. [23] and Dang and Hihara [26] conducted numerical modelling to analyse the local heat transfer characteristics in horizontal flows in small diameter tubes. Because the thermophysical properties of CO_2 are significantly dependent on temperature and pressure, conventional turbulence models proposed for constant-property conditions might not be valid for supercritical pressure conditions; this presents difficulties in selecting suitable turbulence models for numerical simulations. Dang and Hihara [26] tested four turbulence models for heating and cooling of supercritical CO_2 flow in tubes, including three low-Reynolds-number k–ε models and one mixing length model. Based on the comparison of results with experimental data [25], they suggested that the JL model (a low-Reynolds-number k–ε model by Jones and Launder) showed the best agreement with the experimental data, while the three other models (a mixing length model by Bellmore and Reid, and two other low-Reynolds-number k–ε models, by Launder and Sharma and Myong and Kasagi) could not effectively reproduce the experimental data. Pitla et al. [23] used the Favre-averaging technique and the k–ε turbulence

model to predict the heat transfer coefficient of cooling supercritical CO_2 flow in a horizontal stainless steel tube of outside diameter 6.35 mm and wall thickness 0.815 mm with water flowing in the outer tube. Comparison between experimental test data and simulation results showed a maximum difference of ±16%. The investigators used curve fits from the experimental and simulation data to propose a correlation for the calculation of the heat transfer correlation for cooling of supercritical CO_2 flow in tubes. Kim et al. [39] also used data from experimental investigations on heat transfer of CO_2 flow in tubes to propose a turbulent heat transfer model based on the superposition of the effect of forced convection, affected by the flow acceleration, and natural convection, induced by buoyancy in the tube. The developed model was claimed to deliver results with a lower mean absolute error in the region of 10% compared to other models.

Most of the studies have been conducted for flows in circular tubes but there have also been studies for non-circular channels such as those employed in printed circuit heat exchangers (PCHEs) and other compact heat exchangers. PCHEs consist of flat metal plates into which fluid flow channels are chemically etched. The etched plates are stacked with alternative hot and cold stream plates and then joined by diffusion bonding to make a heat exchanger block. The developed very compact and higher-integrity core is ideally suited to high pressure and high temperature applications, particularly for CO_2 systems [49, 50]. Kruizenga et al. [30, 31], Li et al. [32] and Ren et al. [38] investigated the heat transfer and pressure drop of CO_2 within PCHEs. Comparison of experimental data with standard correlations for circular tubes showed significant differences near the pseudo-critical temperature region, while modelling predictions using computational fluid dynamics (CFD) and the SST k–ε turbulence model showed good agreement between experimental and simulation results of heat transfer near the pseudo-critical region. Lee and Kim [51] also recommended the SST k–ε turbulence model to investigate the thermohydraulic performance of supercritical CO_2 flowing in PCHEs, because the SST model can combine the advantages of the k–ε and k–ω models with blending functions. Lee et al. [35] performed experiments to investigate the heat transfer characteristics of CO_2 at supercritical pressure in a micro-fin tube gas cooler during cooling. They found that the cooling heat transfer coefficient of the micro-fin tube increased by between 12% and 39% over that for a same diameter smooth tube at the same conditions. Comparison of experimental results with the results estimated from published correlations, showed that the experimental data yielded a higher heat transfer coefficient compared to those from correlations. The difference was more pronounced close to the critical temperature.

3.2 Vertical channels

A summary of studies on the thermohydraulic performance of CO_2 at supercritical pressure flowing inside vertical channels is presented in Table 3 in chronological order. The investigated factors influencing heat transfer are detailed in Table 4. In vertical channels, the effects of buoyancy on heat transfer is much more significant for CO_2 at supercritical pressure due to axial density gradients, radial differences in viscosity and rapid changes of density in the flow. A summary of the results of important studies is given below.

Bourke et al. [52], Liao and Zhao [22], Pidaparti et al. [36] and Zhang et al. [73] performed experimental investigations with both vertically upward and downward flow to determine the effect of buoyancy under heating conditions. They all found that buoyancy effects were significant for both upward and downward flow at Reynolds numbers up to 10^5. Bourke et al. [52] and Pidaparti et al. [36] reported that buoyancy effects could enhance heat transfer for downward flow while Liao and Zhao [22] showed that the buoyancy effects could enhance heat transfer for upward flow but reduce it in downward flow. Fig. 4 shows the data from Pidaparti et al. [36] for flow in a stainless steel tube of internal diameter 10.9 mm. It can be seen that for the same heat flux, mass flux and inlet pressure, the wall temperature (Fig. 4a) is lower for downward flow compared to upward flow. This is reflected in a higher heat transfer coefficient for downward compared to upward flow (Fig. 4b). It seems that in flows in macro tubes, the turbulent shear stress, enhanced by buoyancy forces, results in an enhancement in heat transfer for downward flow, while the buoyancy force opposes the wall shear stress to reduce the turbulence production, thus leading to a reduction in heat transfer for upward flow. Fig. 5 shows results for heat transfer coefficient in microtubes for both upward and downward flow presented by Liao and Zhao [22]. Fig. 5a, shows results for internal tube diameter of 0.7 mm, inlet pressure of 80 bar and flow rate of 0.05 kg/min whereas Fig. 5b shows results for a tube diameter of 1.4 mm, inlet pressure of 80 bar and flow rate of 0.1 kg/min. In both cases the heat transfer coefficient is higher for upward flow compared to downward flow at temperatures above approximately 35 ^oC. It seems that in microchannels, the free convection effect in upward flow has a stronger influence than the influence of buoyancy in downward flow. It can also be seen that increasing the tube diameter from 0.7 mm to 1.4 mm and the flow rate from 0.5 to 1.0 kg/min increases substantially the heat transfer coefficient. He et al. [54, 55] simulated turbulent-convection heat transfer of CO_2 flow in a vertical tube of diameter 0.948 mm and showed that the buoyancy effect was generally insignificant

in mini/micro-tubes. The heat transfer can still be significantly impaired by flow acceleration when the heating was strong, leading to a reduction in turbulence production. Kim and Kim [70] experimentally investigated heat transfer characteristics in a supercritical vertical upward CO_2 flow. Their analysis indicated that the flow acceleration and significant specific heat variation in the boundary layer greatly influenced the heat transfer phenomena under the tested experimental conditions.

Jiang et al. [60, 61, 62] experimentally and numerically investigated convection heat transfer of CO_2 at supercritical pressure in vertical mini-tubes with diameters from 0.1 mm to 1.59 mm. Their results showed that for mini-tubes such as the one with inside diameter of 0.27 mm, the buoyancy effect was quite small, but the flow acceleration due to heating for these conditions strongly reduced the heat transfer for high heat fluxes. Jiang et al. [53, 56, 63] experimentally investigated convection heat transfer of CO_2 at supercritical pressure in vertical porous tubes. They concluded that the variable thermophysical properties of CO_2 and the buoyancy significantly influenced the convection heat transfer in the vertical mini-tubes and in the porous media and the convection heat transfer in the porous tubes was very different from that in empty tube. The convection heat transfer coefficient in the porous media increased with increasing heat flux due to the acceleration of the fluid flow in the porous media. Buoyancy resulted in different variations of local heat transfer coefficients for upward and downward flows, but when the wall temperatures were much higher than the pseudo-critical temperature, the local heat transfer coefficients along the porous tube decreased continuously for both upward and downward flows.

Xu et al. [72] experimentally examined the turbulent convection heat transfer of CO_2 in straight and serpentine vertical mini-tubes. Infrared temperature measurement was used to measure the distribution of the wall temperature. The effects of variations in thermophysical properties, and the integrated effects of the buoyancy and centrifugal force were analysed by comparing the heat transfer performance between the upward and the downward flow in a serpentine tube and a straight tube under similar experimental conditions. Results showed that the heat transfer performance was better in the serpentine tube than the straight tube because of the secondary flow attributable to centrifugal forces. At the relatively low buoyancy number $Bo^* = \frac{Gr^*}{Re^{3.425}Pr^{0.8}}$ proposed by Jackson et al. [76], the heat transfer in the serpentine vertical tube for downward flow performed better than upward flow due to the effect of gravitational buoyancy on the intensity of turbulence. At relatively

high *Bo** number, the turbulent-convection heat transfer in the serpentine vertical tube performed better for upward flow than for downward flow with no heat transfer deterioration occurring in the serpentine vertical tube.

Kim et al. [57] measured wall-temperature variations of vertical tubes with circular, triangular, and square cross-sections to identify the effect of the cross-sectional shape on the CO_2 heat transfer. They compared wall-temperature distributions in the streamwise direction at the same heat flux and mass velocity conditions and found that the non-circular tubes along the heating region showed a similar trend to the circular tubes but with earlier peaks of wall temperature, due to the different heating areas for the three different tubes. Kim et al. [59, 64] and Bae and Kim [65] also carried out a series of experiments in narrow annulus passages of a concentric and eccentric layout with the aim of collecting heat transfer data to provide an empirical heat transfer correlation required for a supercritical-pressure water-cooled reactor design. They found that heat transfer deterioration occurred at lower mass fluxes if the heat flux increases beyond a certain value; comparison with the tube-test results showed that the degree of heat transfer deterioration was smaller. They attributed this suppression of heat transfer deterioration to a different mechanism for heat transfer deterioration than that of the tube: they determined that the interaction of a wall frictional force and a buoyancy force affects the cross-sectional velocity profile.

3.3 Helical coils

A summary of studies on the thermohydraulic performance of CO_2 at supercritical pressure flowing inside helical coils is shown in Table 5, and the investigated factors influencing heat transfer are indicated in Table 6. The effects of buoyancy on heat transfer are also significant for CO_2 due to axial density gradients, radial differences in viscosity and rapid changes in density in the flow and will be emphasized here.

Zhang et al. [77] experimentally investigated the mixed convective heat transfer of CO_2 at supercritical pressures inside a vertical helically coiled tube under constant-heat-flux conditions. Experiments were conducted at three supercritical pressures for various heat and mass fluxes. They found that the coupling effects of the buoyancy force, centrifugal force, and variations in the physical properties determined the temperature and heat transfer coefficient distributions along the circumference of the tube. The secondary flow induced by the centrifugal force during forced convection, the secondary flow resulting from the buoyancy force during

mixed convection, and the large heat capacity near the pseudo-critical temperature led to heat transfer enhancement. Weakening of the secondary flow and a reduction in the thermal conductivity result in heat transfer deterioration.

Wang et al. [78, 79] and Liu et al. [80, 81] investigated experimentally and numerically the influence of heat flux, pressure and mass flux on the flow and heat transfer, of CO_2 flow in helically coiled tubes of different diameters. It has been found that increasing the mass flux leads to an increase in the heat transfer coefficient. A reduction in pressure also increases the heat transfer coefficient slightly [80] but the heat flux has no influence below the critical point and only a small effect above it. Increase of the heat flux in the pseudo-critical region and above causes a small reduction in the heat transfer coefficient. It was also found that reducing the diameter of the tube in the range 2-4 mm resulted in a significant increase in the heat transfer coefficient across the whole range of the fluid bulk temperature 20-50 ^{o}C. There was no difference in the heat transfer coefficient between cooling and heating below the critical point. However, cooling resulted in a higher heat transfer coefficient in the pseudo-critical region and above with the conclusion that the buoyancy effect has limited impact on the cooling heat transfer coefficient.

4. Empirical correlations of heat transfer to CO_2 at supercritical pressure

Until now, satisfactory analytical methods have not been developed for CO_2 at supercritical pressure due to the difficulty in dealing with the abrupt thermophysical variations of the CO_2 in the pseudo-critical region. Most of the empirical heat transfer correlations are based on the conventional single-phase in-tube forced-convection heat transfer correlation by modifying the effect of variable physical properties near the critical point with a function. The basic used for developing the heat transfer empirical correlations of CO_2 at supercritical pressure are summarized below.

(1) Dittus–Boelter correlation [82]:

$$Nu_{\mathrm{b}} = 0.023 Re_{\mathrm{b}}^{0.8} Pr_{\mathrm{b}}^{n} \quad (1)$$

where n = 0.4 for heating and n = 0.3 for cooling.

(2) Petukhov and Kirillov correlation [83]:

$$Nu_{\mathrm{b}} = \frac{(\xi/8)Re_{\mathrm{b}}\overline{Pr}_{\mathrm{b}}}{12.7\sqrt{\xi/8}\left(\overline{Pr}_{\mathrm{b}}^{2/3} - 1\right) + 1.07} \tag{2}$$

$$\xi = \frac{1}{(1.82\log_{10}Re_{\mathrm{b}} - 1.64)^2} \tag{3}$$

$$\overline{Pr}_{\mathrm{b}} = \frac{\overline{c_{\mathrm{p}}}}{h_{\mathrm{out}} - h_{\mathrm{in}}}\int_{h_{\mathrm{in}}}^{h_{\mathrm{out}}}\frac{\mu(h)}{k(h)}dT, \overline{c_{\mathrm{p}}} = (h_{\mathrm{b}} - h_{\mathrm{w}})/(T_{\mathrm{b}} - T_{\mathrm{w}}) \tag{4}$$

(3) Gnielinski correlation [84]:

$$Nu_{\mathrm{b}} = \frac{(\xi/8)(Re_{\mathrm{b}} - 1{,}000)Pr_{\mathrm{b}}}{1 + 12.7\sqrt{\xi/8}\left(Pr_{\mathrm{b}}^{2/3} - 1\right)} \tag{5}$$

Summaries of the empirical heat transfer correlations for CO_2 at supercritical pressure flowing inside channels are presented in Tables 7, 8 and 9, respectively, corresponding to modification of the Dittus–Boelter, Petukhov and Kirillov and Gnielinski correlations. All the correlations were proposed or developed based only on CO_2 at supercritical pressure data. The correlations proposed by Liao and Zhao [17, 22], Yoon et al. [24], Son et al. [28], Kim et al. [57], and Lee et al. [35] are modification of the Dittus–Boelter correlation; the correlations proposed by Krasnoshchekov and Protopopov [86] and Krasnoshchekov [87], are modifications of the Petukhov and Kirillov correlation, and the correlations proposed by Pitla et al. [23] and Dang and Hihara [25] are modifications of the Gnielinski correlation.

Alongside the above three correlations, Kim et al. [59], Bae and Kim. [65], Bruch et al. [67], Li et al. [68], Bae et al. [70] and Li et al. [34], introduced modifications to the Jackson correlation [88] using CO_2 data obtained from experimental investigations. These correlations are listed in Table 10. Jackson's correlation [88] was proposed for supercritical nuclear reactor cooling using water based on review of existing literature and data. Details of the correlations are given below:

$$Nu_{\mathrm{b}} = 0.0183Re_{\mathrm{b}}^{0.82}Pr_{\mathrm{b}}^{0.5}\left(\frac{\rho_{\mathrm{w}}}{\rho_{\mathrm{b}}}\right)^{0.3}\left(\frac{\overline{c_{\mathrm{p}}}}{c_{\mathrm{pb}}}\right)^{n} \tag{6}$$

$$\overline{c_{\mathrm{p}}} = (h_{\mathrm{b}} - h_{\mathrm{w}})/(T_{\mathrm{b}} - T_{\mathrm{w}}) \tag{7}$$

$n = 0.4$, for $T_{\mathrm{b}} < T_{\mathrm{w}} < T_{\mathrm{pc}}) \leq 1$ or $1.2T_{\mathrm{pc}} < T_{\mathrm{b}} < T_{\mathrm{w}}$ (8)

$n = 0.4 + 0.2\ ((T_{\mathrm{w}} / T_{\mathrm{pc}}) - 1)$, for $T_{\mathrm{b}} < T_{\mathrm{pc}} < T_{\mathrm{w}}$ (9)

$n = 0.4 + 0.2\ ((T_{\mathrm{w}} / T_{\mathrm{pc}}) - 1)(1 - 5(T_{\mathrm{b}} / T_{\mathrm{pc}}) - 1\ )$, for $T_{\mathrm{pc}} < < 1.2T_{\mathrm{pc}}$ or $T_{\mathrm{b}} < T_{\mathrm{w}}$ (10)

where T_{b}, T_{pc}, and T_{w} are in Kelvin.

In Tables 7-10, we provide as much of the necessary information as possible for the calculation of heat transfer coefficients for CO_2 flow at supercritical pressures. However, it should be pointed out that all the correlations presented, require both bulk and wall temperature to calculate the thermophysical properties and most of them were proposed based on the investigators' own experimental data at specific operating conditions. This makes it difficult to compare the available correlations against most of the independent experimental data, making it particularly challenging to propose a unique, universal, correlation over a wide range of test parameters using appropriate measurement and data-reduction methods. Chai and Tassou [89] employed three-dimensional CFD models to investigate the heat transfer and pressure drop characteristics of CO_2 at supercritical pressure in mini-channels and compared their simulation results with six empirical correlations as shown Fig. 6. Three of the correlations are the traditional ones for turbulent flow in circular tubes, including Dittus-Boelter correlation [82], the Sieder and Tate correlation [90] and the Gnielinski correlation [84]. The other three correlations are particularly relevant to heat transfer of CO_2 in horizontal tubes and are: the Krasnoshchekov [87], the Pitla et al. correlation [23] and the Dang and Hihara correlation [25]. For heating conditions, the Krasnoshchekov and Protopopov correlation showed the best prediction with a difference with CFD simulation results of less than 5%, not including the entrance effect. For cooling, the Krasnoshchekov and Protopopov correlation also provided good agreement with CFD results at pressure 150 bar. However, none of the empirical correlations provided good prediction compared with the results of CFD simulation at pressures close to the critical point [89]. To date, to the knowledge of the authors, there is no universally accepted friction factor correlation for CO_2 in the critical and pseudo-critical region. Chai and Tassou [89] compared the local friction factor from CFD simulations with the Blasius correlation ($f = 0.3164 / Re^{0.25}$) and the Petukhov correlation [83]. For the heating mode, both correlations were found to predict the friction factor well for the pressure of 150 bar, and underpredict it by 16-18% for the pressure of 75 bar. For the cooling mode, the two correlations overpredicted the friction factor by 15-43% compared to the CFD results for the 75 bar pressure and by 0-15% for the 150 bar pressure.

5. Conclusions and recommendations

A review of heat transfer of CO_2 at supercritical pressure in the critical and pseudo-critical region is presented for different channel geometries (smooth tubes, porous tubes, concentric annular passages, micro-fin tubes and

helical coils) with hydraulic diameters from 0.27 to 22.8 mm and covering bulk temperature from 0 to 120 ^{o}C and pressure from 74 to 150 bar. Detailed comparisons and analysis of available heat transfer correlations for CO_2 at supercritical pressure are discussed. The following conclusions can be drawn:

(1) Due to the significant variation of thermophysical properties of CO_2 in the near-critical-point region, the heat transfer characteristics of CO_2 are quite different from other regions. In particular, with the sudden increase of specific heat near the critical region, the heat transfer coefficient increases significantly. reaching its peak at the pseudo-critical temperature. Due to the density change, buoyancy influences heat transfer in all the flow orientations. Heat transfer can also be impaired by flow acceleration, especially for high-heat-flux conditions and in mini/micro channels.

(2) The majority of publications are related to heat transfer in circular tubes, while very few publications are devoted to non-circular channels. The heat transfer and pressure drop characteristics of CO_2 at supercritical pressure are influenced by many geometry and operation parameters, including channel shape and dimension, mass flux, heat flux, bulk temperature, pressure, flow direction, tube diameter and buoyancy, and heating or cooling mode. Larger CO_2 mass flux, and bulk temperature close to the pseudo-critical point usually lead to a higher heat transfer coefficient and pressure drop. The influence of pressure and heat flux are more complicated, and different for heating or cooling modes and for bulk temperature below or above the pseudo-critical point.

(3) The effect of heat flux on the heat transfer coefficient is significantly different between heating and cooling modes: particularly important in heating mode while negligible impact in cooling mode. The deterioration under heating mode is mainly caused by the wall temperature profile. An earlier peak of the wall temperature leads to the distortion of shear stress and reduction of turbulent production due to the sharp variations of CO_2 thermophysical properties. Fundamental understanding of the complex phenomenon of heat transfer deterioration in heating mode is recommended to be investigated.

(4) Buoyancy forces in large channels lead to enhanced heat transfer for downward flow and a reduction for upward flow. The free convection effect in mini or micro channels can become stronger and suppress buoyancy effects to lead to enhancement of heat transfer for upward flow. Therefore, buoyancy force is significant in large tubes while generally insignificant in mini/micro channels. The influence of buoyancy on heat transfer is much more significant in vertical rather than horizontal flows in channels.

This is largely due to the influence of axial density gradients, radial differences in viscosity and rapid changes in density in vertical flows. The influence of buoyancy effects with tube dimension is less investigated and further research is needed in this area for the development of universal empirical correlations for the design of CO_2 heat exchangers for different applications.

(5) Several authors have developed empirical correlations for specific geometries; however, most of these have been developed for a given range of temperature, pressure, heat flux, and flow characteristics. Comparisons of various correlations of heat transfer for CO_2 at supercritical pressure showed that several correlations can be used for preliminary estimation of heat transfer in tubes, but no one correlation is able to accurately describe local heat transfer for different channel geometries. It is recommended that further unique universal correlations be developed, over a wide range of test parameters, employing appropriate measurement and data-reduction methods. To realize this, further efforts should be made to develop accurate and repeatable methods for local heat transfer measurement. Heat exchanger optimization is also an important field, and requires specific attention not only for the individual heat exchanger but also the system as a whole. The available studies do not cover as wide a range of operating conditions as is required for different applications and, therefore, new experimental and numerical data should be produced over a wider range of test parameters.

Acknowledgements

The work presented in this paper is supported by a number of funders as follows: i) The Engineering and Physical Sciences Research Council (EPSRC) of the UK under research grant EP/V001795/1 – SCOTWOHR and ii) the European Union's Horizon 2020 research and innovation programme under grant agreement No. 680599 – I-ThERM and Grant Agreement No. 101022831 – CO2OLHEAT. The authors would like to acknowledge the financial support received from the funders and industry partners. All data used are in the paper but if any additional information is required it can be obtained by contacting the corresponding author.

References

[1] Austin, B. T., Sumathy, K., Transcritical carbon dioxide heat pump systems: A review, *Renewable and Sustainable Energy Reviews*, vol. 15, no. 8, pp. 4013-4029, 2011.

[2] Nekså, P., CO_2 heat pump systems, *International Journal of Refrigeration*, vol. 25, no. 4, pp. 421-427, 2002.

[3] Cheng, L., Xia, G., Li, Q., CO_2 Evaporation Process Modeling: Fundamentals and Engineering Applications, *Heat Transfer Engineering*, pp. 1-28, 2021.

[4] Suamir, I. N., Tassou, S. A., Performance evaluation of integrated trigeneration and CO_2 refrigeration systems, *Applied Thermal Engineering*, vol. 50, no. 2, pp. 1487-1495, 2013.

[5] Chai, L., Tsamos, K. M., Tassou, S. A., Modelling and evaluation of the thermohydraulic performance of finned-tube supercritical carbon dioxide gas coolers, *Energies*, vol. 13, no. 5, pp. 1031, 2020.

[6] Ahn, Y., Bae, S. J., Kim, M., Review of supercritical CO_2 power cycle technology and current status of research and development, *Nuclear Engineering and Technology*, vol. 47, no. 6, pp. 647-661, 2015.

[7] Zhang, J. F., Qin, Y., Wang, C. C., Review on CO_2 heat pump water heater for residential use in Japan, *Renewable and Sustainable Energy Reviews*, vol. 50, pp. 1383-1391, 2015.

[8] Bensafi, A., Thonon, B., Transcritical R744 (CO_2) heat pumps, Technician's Manual, CETIAT, Villeurbanne, Manual, 2007.

[9] Bamigbetan, O., Eikevik, T. M., Nekså, P., Review of vapour compression heat pumps for high temperature heating using natural working fluids, *International Journal of Refrigeration*, vol. 80, pp. 197-211, 2017.

[10] Chai, L., Tassou, S. A., A review of printed circuit heat exchangers for helium and supercritical CO_2 Brayton cycles, *Thermal Science and Engineering Progress*, vol. 18, pp. 100543, 2020.

[11] Marchionni, M., Bianchi, G., Tassou, S. A., Review of supercritical carbon dioxide (sCO_2) technologies for high-grade waste heat to power conversion, *SN Applied Sciences*, vol. 2, no. 4, pp. 1-13, 2020.

[12] White, M. T., Bianchi, G., Chai, L., Review of supercritical CO_2 technologies and systems for power generation, *Applied Thermal Engineering*, vol. 185, pp. 116447, 2021.

[13] Chai, L., Tassou, S. A., Modelling and evaluation of the thermohydraulic performance of compact recuperative heat exchangers in supercritical carbon dioxide waste heat to power conversion systems, *Heat Transfer Engineering*, pp. 1-17, 2021.

[14] Pioro, I. L., Khartabil, H. F., Duffey, R. B., Heat transfer to supercritical fluids flowing in channels—empirical correlations (survey), *Nuclear engineering and design*, vol. 230, no. 1, pp. 69-91, 2004.

[15] Pioro, I. L., Duffey, R. B., Experimental heat transfer in supercritical water flowing inside channels (survey), *Nuclear engineering and design*, vol. 235, no. 22, pp. 2407-2430, 2005.

[16] Lemmon, E. W., Huber, M. L., McLinden, M. O., NIST Standard Reference Database 23: Reference Fluid Thermodynamic and Transport Properties - REFPROP, Version 9.1, National Institute of Standards and Technology, Gaithersburg, MD, USA, 2013.

[17] Liao, S. M., Zhao, T. S., Measurements of heat transfer coefficients from supercritical carbon dioxide flowing in horizontal mini/micro channels, *Transactions of the American Society of Mechanical Engineers Journal of Heat Transfer*, vol. 124, no. 3, pp. 413-420, 2002.

[18] Cabeza, L. F., de Gracia, A., Fernández, A. I., Supercritical CO_2 as heat transfer fluid: A review, *Applied Thermal Engineering*, vol. 125, pp. 799-810, 2017.

[19] Cheng, L., Ribatski, G., Thome, J. R., Analysis of supercritical CO_2 cooling in macro- and micro-channels, *International Journal of Refrigeration*, vol. 31, no. 8, pp. 1301-1316, 2008.

[20] Schnurr, N. M., Heat transfer to carbon dioxide in the immediate vicinity of the critical point, *Journal of Heat Transfer*, vol. 91, no. 1, pp. 16-20, 1969.

[21] Adebiyi, G. A., Hall, W. B., Experimental investigation of heat transfer to supercritical pressure carbon dioxide in a horizontal pipe, *International Journal of Heat and Mass Transfer*, vol. 19, no. 7, pp. 715-720, 1976.

[22] Liao, S. M., Zhao, T. S., An experimental investigation of convection heat transfer to supercritical carbon dioxide in miniature tubes, *International Journal of Heat and Mass Transfer*, vol. 45, no. 25, pp. 5025-5034, 2002.

[23] Pitla, S. S., Groll, E. A., Ramadhyani. S., New correlation to predict the heat transfer coefficient during in-tube cooling of turbulent supercritical CO_2, *International Journal of Refrigeration*, vol. 25, no. 7, pp. 887-895, 2002.

[24] Yoon, S. H., Kim, J. H., Hwang, Y. W., Heat transfer and pressure drop characteristics during the in-tube cooling process of carbon dioxide in the supercritical region, *International Journal of Refrigeration*, vol. 26, no. 8, pp. 857-864, 2003.

[25] Dang, C., Hihara, E., In-tube cooling heat transfer of supercritical carbon dioxide. Part 1. Experimental measurement, *International Journal of Refrigeration*, vol. 27, no. 7, pp. 736-747, 2004.

[26] Dang, C., Hihara, E., In-tube cooling heat transfer of supercritical carbon dioxide. Part 2. Comparison of numerical calculation with different turbulence models, *International Journal of Refrigeration*, vol. 27, no. 7, pp. 748-760, 2004.

[27] Huai, X. L., Koyama, S., Zhao, T. S., An experimental study of flow and heat transfer of supercritical carbon dioxide in multi-port mini channels under cooling conditions, *Chemical Engineering Science*, vol. 60, no. 12, pp. 3337-3345, 2005.

[28] Son, C. H., Park, S. J., An experimental study on heat transfer and pressure drop characteristics of carbon dioxide during gas cooling process in a horizontal tube, *International Journal of Refrigeration*, vol. 29, no. 4, pp. 539-546, 2006.

[29] Yun, R., Hwang, Y., Radermacher, R., Convective gas cooling heat transfer and pressure drop characteristics of supercritical CO_2/oil mixture in a minichannel tube, *International Journal of Heat and Mass Transfer*, vol. 50, no. 23, pp. 4796-4804, 2007.

[30] Huai, X., Koyama, S., Heat transfer characteristics of supercritical CO_2 flow in small-channeled structures, *Experimental Heat Transfer*, vol. 20, no. 1, pp. 19-33, 2007.

[31] Oh, H. K., Son, C. H., New correlation to predict the heat transfer coefficient in-tube cooling of supercritical CO_2 in horizontal macro-tubes, *Experimental Thermal and Fluid Science*, vol. 34, no. 8, pp. 1230-1241, 2010.

[32] Kruizenga, A., Anderson, M., Fatima, R., Heat transfer of supercritical carbon dioxide in printed circuit heat exchanger geometries, *Journal of Thermal Science and Engineering Applications*, vol. 3, no. 3, pp. 031002, 2011.

[33] Kruizenga, A., Li, H., Anderson, M., Supercritical carbon dioxide heat transfer in horizontal semi-circular channels, *Journal of Heat Transfer*, vol. 134, no. 8, pp. 081802, 2012.

[34] Li, H., Kruizenga, A., Anderson, M., Development of a new forced convection heat transfer correlation for CO_2 in both heating and cooling modes at supercritical pressures, *International Journal of Thermal Sciences*, vol. 50, no. 12, pp. 2430-2442, 2011.

[35] Lee, H. S., Kim, H. J., Yoon, J. I., The cooling heat transfer characteristics of the supercritical CO_2 in micro-fin tube, *Heat Mass Transfer*, vol. 49, no. 2, pp. 173-184, 2013.

[36] Pidaparti, S. R., McFarland, J. A., Mikhaeil, M. M., Investigation of buoyancy effects on heat transfer characteristics of supercritical carbon dioxide in heating mode, *Journal of Nuclear Engineering and Radiation Science*, vol. 1, no. 3, pp. 031001, 2015.

[37] Tanimizu, K., Sadr, R., Experimental investigation of buoyancy effects on convection heat transfer of supercritical CO_2 flow in a horizontal tube, *Heat Mass Transfer*, vol. 52, no. 4, pp. 713-726, 2016.

[38] Wang, J., Guo, P., Yan, J., Experimental study on forced convective heat transfer of supercritical carbon dioxide in a horizontal circular tube under high heat flux and low mass flux conditions, *Advances in Mechanical Engineering*, vol. 11, no. 3, pp. 168781401983080, 2019.

[39] Kim, T. H., Kwon, J. G., Park, J. H., Heat transfer model for horizontal flows of CO_2 at supercritical pressures in terms of mixed convection, *International journal of heat and mass transfer*, vol. 131, pp. 1117-1128, 2019.

[40] Ren, Z., Zhao, C. R., Jiang, P. X., Investigation on local convection heat transfer of supercritical CO_2 during cooling in horizontal semi-circular channels of printed circuit heat exchanger, *Applied Thermal Engineering*, vol. 157, pp. 113697, 2019.

[41] Zhang, S., Xu, X., Liu, C., Experimental and numerical comparison of the heat transfer behaviors and buoyancy effects of supercritical CO_2 in various heating tubes, *International Journal of Heat and Mass Transfer*, vol. 149, pp. 119074, 2020.

[42] Wang, L., Pan, Y. C., Der Lee, J., Experimental investigation in the local heat transfer of supercritical carbon dioxide in the uniformly heated horizontal miniature tubes, *International Journal of Heat and Mass Transfer*, vol. 159, pp. 120136, 2020.

[43] Wang, L., Pan, Y. C., Der Lee, J., Experimental investigation in the pressure drop characteristics of supercritical carbon dioxide in the uniformly heated horizontal miniature tubes, *The Journal of Supercritical Fluids*, vol. 162, pp. 104839, 2020.

[44] Guo, P., Liu, S., Yan, J., Experimental study on heat transfer of supercritical CO_2 flowing in a mini tube under heating conditions, *International Journal of Heat and Mass Transfer*, vol. 153, pp. 119623, 2020.

[45] Wahl, A., Mertz, R., Laurien, E., Heat transfer correlation for sCO_2 cooling in a 2 mm tube, *The Journal of Supercritical Fluids*, vol. 173, pp. 105221, 2021.

[46] Park, J. H., Kim, M. H., Modeling of local heat transfer on supercritical pressure CO_2 in horizontal semi-circular tube, *International Journal of Heat and Mass Transfer*, pp. 122197, 2021.

[47] Ehsan, M. M., Guan, Z., Klimenko, A. Y., A comprehensive review on heat transfer and pressure drop characteristics and correlations with supercritical CO_2 under heating and cooling applications, *Renewable and Sustainable Energy Reviews*, vol. 92, pp. 658-675, 2018.

[48] Jackson, J. D., Some striking features of heat transfer with fluids at pressures and temperatures near the critical point, Keynote Paper for International Conference on Energy Conversion and Application (ICECA '2001), Wuhan, China, 2001.

[49] Chu, W., Li, X., Chen, Y., Experimental study on small scale printed circuit heat exchanger with zigzag channels, *Heat Transfer Engineering*, vol. 42, no. 9, pp. 723-735, 2021.

[50] Naderi, C., Rasouli, E., Narayanan, V., Design and Performance of a Microchannel Supercritical Carbon Dioxide Recuperator with Integrated Header Architecture, *Journal of Enhanced Heat Transfer*, vol. 26, no. 4, pp. 65–392, 2019.

[51] Lee, S. M., Kim, K. Y., A parametric study of the thermal-hydraulic performance of a zigzag printed circuit heat exchanger, *Heat transfer engineering*, vol. 35, no. 13, pp. 1192-1200, 2014.

[52] Bourke, P. J., Pulling, D. J., Gill, L. E., Forced convective heat transfer to turbulent CO_2 in the supercritical region, *International Journal of Heat and Mass Transfer*, vol. 13, no. 8, pp. 1339-1348, 1970.

[53] Jiang, P. X., Xu, Y. J., Lv, J., Experimental investigation of convection heat transfer of CO_2 at super-critical pressures in vertical mini-tubes and in porous media, *Applied Thermal Engineering*, vol. 24, no. 8, pp. 1255-1270, 2004.

[54] He, S., Kim, W. S., Jiang, P. X., Simulation of mixed convection heat transfer to carbon dioxide at supercritical pressure. *Proceedings of the Institution of Mechanical Engineers, Part C: Journal of Mechanical Engineering Science*, vol. 218, no. 11, pp. 1281-1296, 2004.

[55] He, S., Jiang, P. X., Xu, Y. J., A computational study of convection heat transfer to CO_2 at supercritical pressures in a vertical mini tube, *International Journal of Thermal Sciences*, vol. 44, no. 6, pp. 521-530, 2005.

[56] Jiang, P. X., Shi, R. F., Xu, Y. J., Experimental investigation of flow resistance and convection heat transfer of CO_2 at supercritical pressures in a vertical porous tube, *The Journal of Supercritical Fluids*, vol. 38, no. 3, pp. 339-346, 2006.

[57] Kim, J. K., Jeon, H. K., Lee, J. S., Wall temperature measurement and heat transfer correlation of turbulent supercritical carbon dioxide flow in vertical circular/non-circular tubes, *Nuclear Engineering and Design*, vol. 237, no. 15, pp. 1795-1802, 2007.

[58] Kim, H. Y., Kim, H., Song, J. H., Heat transfer test in a vertical tube using CO_2 at supercritical pressures, *Journal of Nuclear Science and Technology*, vol. 44, no. 3, pp. 285-293, 2007.

[59] Kim, H. Y., Kim, H., Kang, D. J., Experimental investigations on a heat transfer to CO_2 flowing upward in a narrow annulus at supercritical pressures, *Nuclear Engineering and Technology*, vol. 40, no. 2, pp. 155-162, 2008.

[60] Jiang, P. X., Zhang, Y., Zhao, C. R., Convection heat transfer of CO_2 at supercritical pressures in a vertical mini tube at relatively low Reynolds numbers, *Experimental Thermal and Fluid Science*, vol. 32, no. 8, pp. 1628-1637, 2008.

[61] Jiang, P. X., Zhang, Y., Xu, Y. J., Experimental and numerical investigation of convection heat transfer of CO_2 at supercritical pressures in a vertical tube at low Reynolds numbers, *International Journal of Thermal Sciences*, vol. 47, no. 8, pp. 998-1011, 2008.

[62] Jiang, P. X., Zhang, Y., Shi, R. F., Experimental and numerical investigation of convection heat transfer of CO_2 at supercritical pressures in a vertical mini-tube, *International Journal of Heat and Mass Transfer*, vol. 51, no. 11, pp. 3052-3056, 2008.

[63] Jiang, P. X., Shi, R. F., Zhao, C. R., Experimental and numerical study of convection heat transfer of CO_2 at supercritical pressures in vertical porous tubes, *International Journal of Heat and Mass Transfer*, vol. 51, no. 25, pp. 6283-6293, 2008.

[64] Kim, H., Kim, H. Y., Song, J. H., Heat transfer to supercritical pressure carbon dioxide flowing upward through tubes and a narrow annulus passage, *Progress in Nuclear Energy*, vol. 50, no. 2, pp. 518-525, 2008.

[65] Bae, Y. Y., Kim, H. Y., Convective heat transfer to CO_2 at a supercritical pressure flowing vertically upward in tubes and an annular channel, *Experimental Thermal and Fluid Science*, vol. 33, no. 2, pp. 329-339, 2009.

[66] Cho, B. H., Kim, Y. I., Bae, Y. Y., Prediction of a heat transfer to CO_2 flowing in an upward path at a supercritical pressure, *Nuclear Engineering and Technology*, vol. 41, no. 7, pp. 907-920, 2009.

[67] Bruch, A., Bontemps, A., Colasson, S., Experimental investigation of heat transfer of supercritical carbon dioxide flowing in a cooled vertical tube, *International Journal of Heat and Mass Transfer*, vol. 52, no. 11, pp. 2589-2598, 2009.

[68] Li, Z, H., Jiang, P. X., Zhao, C. R., Experimental investigation of convection heat transfer of CO_2 at supercritical pressures in a vertical circular tube, *Experimental Thermal and Fluid Science*, vol. 34, no. 8, pp. 1162-1171, 2010.

[69] Bae, Y. Y., Kim, H. Y., Kang, D. J., Forced and mixed convection heat transfer to supercritical CO_2 vertically flowing in a uniformly-heated circular tube, *Experimental Thermal and Fluid Science*, vol. 34, no. 8, pp. 1295-1308, 2010.

[70] Kim, D. E., Kim, M. H., Experimental study of the effects of flow acceleration and buoyancy on heat transfer in a supercritical fluid flow in a circular tube, *Nuclear Engineering and Design*, vol. 240, no. 10, pp. 3336-3349, 2010.

[71] Zahlan, H., Groeneveld, D., Tavoularis, S., Measurements of convective heat transfer to vertical upward flows of CO_2 in circular tubes at near-critical and supercritical pressures, *Nuclear Engineering and Design*, vol. 289, pp. 92-107, 2015.

[72] Xu, R. N., Luo, F., Jiang, P. X., Experimental research on the turbulent convection heat transfer of supercritical pressure CO_2 in a serpentine vertical mini tube, *International Journal of Heat and Mass Transfer*, vol. 91, pp. 552-561, 2015.

[73] Zhang, S., Xu, X., Liu, C., Experimental investigation on the heat transfer characteristics of supercritical CO_2 at various mass flow rates in heated vertical-flow tube, *Applied Thermal Engineering*, vol. 157, pp. 113687, 2019.

[74] Zhu, B., Xu, J., Wu, X., Supercritical "boiling" number, a new parameter to distinguish two regimes of carbon dioxide heat transfer in tubes, *International Journal of Thermal Sciences*, vol. 136, pp. 254-266, 2019.

[75] Wang, L., Pan, Y. C., Der Lee, J., Convective heat transfer characteristics of supercritical carbon dioxide in vertical miniature tubes of a uniform heating experimental system, *International Journal of Heat and Mass Transfer*, vol. 167, pp. 120833, 2021.

[76] Jackson, J. D., Hall, W. B., Influences of buoyancy on heat transfer to fluids flowing in vertical tubes under turbulent conditions, Turbulent Forced Convection in Channels and Bundles (1st Edn), Vol. 2, Hemisphere, New York (1979), 613-640.

[77] Zhang, W., Wang, S., Li, C., Mixed convective heat transfer of CO_2 at supercritical pressures flowing upward through a vertical helically coiled tube, *Applied Thermal Engineering*, vol. 88, pp. 61-70, 2015.

[78] Wang, K., Xu, X., Wu, Y., Numerical investigation on heat transfer of supercritical CO_2 in heated helically coiled tubes, *The Journal of Supercritical Fluids*, vol. 99, pp. 112-120, 2015.

[79] Wang, K. Z., Xu, X. X., Liu, C., Experimental and numerical investigation on heat transfer characteristics of supercritical CO_2 in the cooled helically coiled tube, *International Journal of Heat and Mass Transfer*, vol. 108, pp. 1645-1655, 2017.

[80] Liu, X., Xu, X., Liu, C., The effect of geometry parameters on the heat transfer performance of supercritical CO_2 in horizontal helically coiled tube under the cooling condition, *International Journal of Refrigeration*, vol. 106, pp. 650-661, 2019.

[81] Liu, X., Xu, X., Jiao, Y., Flow structure with mixed turbulent flow of supercritical CO_2 heated in helically coiled tube, *Applied Thermal Engineering*, vol. 189, pp. 116684, 2021.

[82] Dittus, F. W., Boelter, L. M. K., University of California publications on engineering, University of California Publications in Engineering, vol. 2, pp. 371, 1930.

[83] Petukhov, B. S., Kirillov, P. L., About heat transfer at turbulent fluid flow in tubes, *Thermal Engineering*, vol. 4, pp. 63-68, 1958.

[84] Gnielinski, V., New equations for heat and mass transfer in turbulent pipe and channel flow, *International Chemical Engineering*, vol. 16, no. 2, pp. 359-368, 1976.

[85] Bringer, R. P., Smith J M. Heat transfer in the critical region, *AIChE Journal*, vol. 3, no. 1, pp. 49-55, 1957.

[86] Krasnoshchekov, E. A., Protopopov, V. S., About heat transfer in flow of carbon dioxide and water at supercritical region of state parameters, *Thermal Engineering*, vol. 310, pp. 94, 1960.

[87] Krasnoshchekov, E. A., Experimental study of heat exchange in carbon dioxide in the supercritical range at high temperature drops (Heat transfer in turbulent carbon dioxide pipeflow at supercritical region), *High Temperature*, vol. 4, pp. 375-382, 1966.

[88] Jackson, J. D., Consideration of the heat transfer properties of supercritical pressure water in connection with the cooling of advanced nuclear reactors, Proceedings of the 13th Pacific Basin Nuclear Conference, Shenzhen City, Shina, October 21–25, 2002.

[89] Chai, L., Tassou, S. A., Effect of cross-section geometry on the thermohydraulic characteristics of supercritical CO_2 in minichannels, *Energy Procedia*, vol. 161, pp. 446-453, 2019.

[90] Sieder, E. N., Tate, G. E., Heat transfer and pressure drop of liquids in tubes, *Industrial & Engineering Chemistry*, vol. 28, no. 12, pp. 1429-1435, 1936.

[91] Jackson, J. D., Fluid flow and convective heat transfer to fluids at supercritical pressure, *Nuclear Engineering and Design*, vol. 264, pp. 24-40, 2013.

Nomenclature

CFD	computational fluid dynamics (CFD)
c_p	specific heat, $J \cdot kg^{-1} K^{-1}$
D_h	hydraulic diameter, m
d	diameter, m
f	formula
G	mass flux, $kg \cdot m^{-2} \cdot s^{-1}$
Gr	Grashof number
g	gravitational acceleration, $m \cdot s^{-2}$
h	heat transfer coefficient, $W \cdot m^{-2} \cdot K^{-1}$; specific enthalpy, $J \cdot kg^{-1}$
k	thermal conductivity, $W \cdot m^{-1} \cdot K^{-1}$
LMTD	log mean temperature difference
m	mass flow rate, $kg \cdot s^{-1}$
NTU	number of transfer unit
Nu	Nusselt number
n	parameter
OD	outer diameter
PCHEs	printed circuit heat exchangers
Pr	Prandtl number
p	pressure, Pa
Q	heat transfer rate, W
q	heat flux, $W \cdot m^{-2}$
Re	Reynolds number
T	temperature, K
T_{pc}	pseudo-critical temperature, K
u	velocity, $m \cdot s^{-1}$
x	length along the channel, m

Δp	pressure drop, Pa
Greek letters	
ρ	density, $kg \cdot m^{-3}$
μ	dynamic viscosity, Pa·s
ν	kinematic viscosity, $m^2 \cdot s^{-1}$
τ	shear stress, Pa
ε	heat transfer effectiveness
ξ	friction factor
Subscripts	
b	bulk fluid
cr	critical
f	film
pc	pseudo-critical
w	wall

Figure and table captions

Fig. 6 Comparison of local heat transfer with empirical correlations [89]: (a) in heating mode and (b) in cooling mode.

Fig. 7 Comparison of local friction factor with empirical correlations [89]: (a) in heating mode and (b) in cooling mode.

Table 1 Summary of heat transfer of CO_2 at supercritical pressure flowing inside horizontal channels.

Reference	**Pressure** ***P*** **(bar)**	**Inlet temperature** ***T*** **(°C)**	**Heat flux** ***q*** **(kW/m^2)**	**Flow rate**	**Working condition**	**Method**	**Flow geometry**
Schnurr [20]	74–77	21 to 38	13-50	*Re*: 8×10^4 to 6.8×10^5	Heating	Experimental	Stainless steel tube with 0.134-inch outer diameter (OD) and 0.015-in-thick walls
Adebiyi and Hall [21]	76	10–31	5–40	*m*: 0.035–0.15 kg/s	Heating	Experimental	Stainless steel tube with 25.4 mm OD and 1.63-mm-thick walls
Liao and Zhao [17]	74–120	Bulk 20–110	10–200	*m*: 0.02–0.2 kg/min *Re*: 10^4–2×10^5	Cooling	Experimental	Six stainless steel circular tubes having diameters of 0.50 mm, 0.70 mm, 1.10 mm, 1.40 mm, 1.55 mm, and 2.16 mm
Liao and Zhao [22]	74–120	Bulk 20–110	10–200	*m*: 0.02–0.2 kg/min *Re*: 10–2×10^5	Heating	Experimental	Stainless steel circular tubes having diameters of 0.70, 1.40, and 2.16 mm
Pitla et al. [23]	84–114	101–124		*m*: 0.02–0.04 kg/s	Cooling	Experimental and numerical	Stainless steel with a nominal OD of 6.35 mm and a wall thickness of 0.815 mm
Yoon et al. [24]	75–88	50–80		*G*: 225–450 kg/(m^2 s)	Cooling	Experimental	Copper tube with an inner diameter of 7.73 mm
Dang and Hihara [25, 26]	80–100	30–70	6–33	*G*: 200–1,200 kg/(m^2 s)	Cooling	Experimental and numerical	Copper tubes with an inner diameter of 1–6 mm

Huai et al. [27]	74–85	22–53	0.8–9	*G*: 113.7–418.6 kg/(m^2 s)	Cooling	Experimental	Multi-port extruded aluminium test section consisting of ten circular channels with an inner diameter of 1.31 mm
Son et al. [28]	75–100	90–100		*G*: 200–400 kg/(m^2 s)	Cooling	Experimental	Stainless steel tube with a nominal OD of 9.53 mm and ID of 7.75 mm
Yun et al. [29]	94	60.5–74.7	20–25	*G*: 200–400 kg/(m^2 s)	Heating	Experimental	Multi-port test section consisting of ten circular channels with an inner diameter of 1.0 mm
Huai and Koyama [30]	75–85	30.48–45.84	1.6–3.3	*G*: 127.1–303.6 kg/(m^2 s)	Cooling	Experimental	Multi-port extruded aluminium test section consisting of ten circular channels with an inner diameter of 1.31 mm
Oh and Son [31]	75–100	90–100		*G*: 200–600 kg/(m^2 s)	Cooling	Experimental	Stainless steel tubes with inside diameter of 4.55 mm and 7.75 mm
Kruizenga et al. [32]	75–81	Bulk 20–100	12–36	*G*: 326–762 kg/(m^2 s)	Cooling	Experimental and numerical	Stainless steel test section with nine semicircular channels of hydraulic diameter of 1.16 mm and length of 0.5 m
Kruizenga et al. [33]	75–102	Bulk 20–100		*G*: 326–1,197 kg/(m^2 s)	Cooling	Experimental and numerical	Stainless steel test section with nine semicircular channels of hydraulic diameter of 1.16 mm and length of 0.5 m
Li et al. [34]	75–100	Bulk 10–90	30	*G*: 326–762 kg/(m^2 s)	Heating and cooling	Experimental and numerical	Stainless steel test section with nine semicircular channels of hydraulic diameter of 1.16 mm and length of 0.5 m

Lee et al. [35]	80–100	100		G: 1,200–2,000 kg/(m^2 s)	Cooling	Experimental	Copper micro-fin tube with inner and outer diameters of 4.6 mm and 5.0 mm, 55 0.2-mm-tall micro-fins with helix angle of 18°
Pidaparti et al. [36]	75–102	20–55	13.5–62.5	G: 150–350 kg/(m^2 s)	Heating	Experimental	Stainless steel tube with inner and outer diameters of 10.9 mm and 12.7 mm
Tanimizu and Sadr [37]	75–90	24–28	16–64	m: 0.011–0.017 g/s	Heating	Experimental	Stainless steel tube with inner and outer diameters of 8.7 mm and 12.7 mm
Wang et al. [38]	76–84	Bulk 20-62	0-200	G: 400–500 kg/(m^2 s) Re: 1.2×10^4–4.3×10^4	Heating	Experimental	Stainless steel tube with a 2 mm inner diameter, 0.5 mm wall thickness, and 100 mm length
Kim et al. [39]	75.86–76.14	13.8–30.1	5.1–26.9	G: 104.34–391.91 kg/(m^2 s)	Heating	Experimental	Stainless steel tube with an inner diameter of 7.75 mm, an electrically heated length of 0.91 m.
Ren et al. [40]	78–81	Bulk 40–100		G: 200–800 kg/(m^2 s)	Cooling	Numerical	Semicircular channels with diameter of 2.8 mm
Zhang et al. [41]	75–90	15	10–70	G: 80–600 kg/(m^2 s)	Heating	Experimental and numerical	Stainless steel tube with an inner diameter of 4 mm and wall thickness of 1 mm.
Wang et al. [42, 43]	76.6–90	30.9–37.3	124.8–130.8	G: 848.8 kg/(m^2 s)	Heating	Experimental	Stainless steel tubes with a fixed outer diameter of 1.6 mm and three inner diameters of 1.0 mm, 0.75 mm and 0. 5 mm.

Guo et al. [44]	76–84 Bulk 20–64		100–200	G: 400-700 kg/(m^2 s)	Heating	Experimental	Stainless steel tube with inner and outer diameters of 2 mm and 3 mm, an effective heated length of 100 mm.
Wahl et al. [45]	77–85	10-40		G: 400–1300 kg/(m^2 s)	Cooling	Experimental and numerical	Cooper tube with inner and outer diameters of 2 mm and 6 mm.
Park and Kim [46]	78	30	13.7-50.3	G: 70–200 kg/(m^2 s)	Heating	Experimental	Semicircular stainless steel tube with hydraulic diameter 4.73 mm, width 7.75 mm and depth 3.88 mm.

Table 2 Investigated factors influencing heat transfer inside horizontal channels.

Reference	Mass flux	Heat flux	Bulk temperature	Pressure	Tube diameter	Buoyancy
Schnurr [20]	√	√	√	√		
Adebiyi and Hall [21]	√	√	√			√
Liao and Zhao [17]	√	√	√	√	√	√
Liao and Zhao [22]	√	√	√	√	√	√
Pitla et al. [23]	√	√	√	√		
Yoon et al. [24]	√	√	√	√		
Dang and Hihara [25, 26]	√	√	√	√	√	
Huai et al. [27]	√	√	√	√		
Son et al. [28]	√	√	√	√		

Yun et al. [29]	√	√	√	√			
Huai and Koyama [30]	√	√	√	√			
Oh and Son [31]	√	√	√	√	√	√	
Kruizenga et al. [32]	√	√	√	√			
Kruizenga et al. [33]	√	√	√	√			
Li et al. [34]	√	√	√	√			
Lee et al. [35]	√	√	√	√			
Pidaparti et al. [36]	√	√	√	√	√	√	
Tanimizu and Sadr [37]	√	√	√	√		√	
Wang et al. [38]	√	√	√	√		√	
Kim et al. [39]	√	√	√	√		√	

Ren et al. [40]	√	√	√	√		√
Zhang et al. [41]	√	√	√	√		√
Wang et al. [42, 43]	√	√	√	√	√	√
Guo et al. [44]	√	√	√	√		√
Wahl et al. [45]	√	√	√	√		√
Park and Kim [46]	√	√	√	√		√

Table 3 Summary of heat transfer of CO_2 at supercritical pressure flowing inside vertical channels.

Reference	**Pressure** ***P*** **(bar)**	**Inlet temperature** ***T*** **(°C)**	**Heat flux** ***q*** **(kW/m^2)**	**Flow rate**	**Working condition**	**Method**	**Flow geometry**
Bourke et al. [52]	74.4–103.2	15–35	6.8–338	*m*: 0.127–0.695 kg/s	Heating	Experimental	Stainless steel tube with inner diameter 22.8 mm and wall thickness 1.27 mm
Liao and Zhao [22]	74–120	Bulk temperature 20–110	10–200	*m*: 0.02–0.2 kg/min *Re*: 10–2×10^5	Heating	Experimental	Stainless steel circular tubes having diameters of 0.70, 1.40, and 2.16 mm
Jiang et al. [53]	95	31–51	45.3–108 in mini-tube and 2.593–28.133 in porous tube	*m*: 1.48–4.17 kg/h in mini-tube and 0.51–1.52 kg/h in porous tube *Re*: 7,810–20,516 in mini-tube and 1,065–3,280 in porous tube	Heating	Experimental	Stainless steel tube with inside and outside diameters of 0.948 mm and 1.729 mm and a copper tube with inside and outside diameters of 4 mm and 6 mm, and one porous circular tube with inside and outside diameters of 4 mm and 6 mm and particle diameters of 0.2–0.28 mm
He et al. [54]	84.6–95.9	8, 10	2.6–15.1	*m*: 0.029–0.082 kg/s	Heating	Numerical	Stainless steel tube with OD of 19 mm and a wall thickness of 1.625 mm
He et al. [55]	84.6–95.9	31–51	10–108	*m*: 1.48–4.17 kg/h	Heating	Numerical	Vertical tube of diameter 0.948 mm
Jiang et al. [56]	77–97	Bulk 22–90	8–92	*m*: 0.5–2 kg/h	Heating	Experimental	Porous cylindrical tube with inside and outside diameters of 4 mm and 6 mm and particle diameters of 0.2–0.28 mm

Kim et al. [57]	80	15–32	5–180	G: 209–1,230 kg/(m^2 s)	Heating	Experimental	Stainless steel tubes with circular, triangular, and square cross-sections, hydraulic diameters of 7.8 mm, 9.8 mm and 7.9 mm
Kim et al. [58]	77.5–88.5	27	20–150	G: 400–1,200 kg/(m^2 s)	Heating	Experimental	Stainless steel tube with inside diameter of 4.4 mm and wall thickness 0.9 mm, vertical
Kim et al. [59]	77.5–81.2	0–37	Up to 150	G: 400–1,200 kg/(m^2 s)	Heating	Experimental	Stainless steel concentric annular passage (ϕ8 mm × ϕ10 mm × L1800 mm)
Jiang et al. [60]	86	30	11.3–113	m: 0.08–0.12 kg/h Re: ≤ 2,900	Heating	Experimental and numerical	Stainless steel tube with inside and outside diameters of 0.27 mm and 1.59 mm, vertical
Jiang et al. [61]	85.8–95.7	20.5 and 33.5	4.49–95	G: 6.29–6.63 kg/(m^2 s) Re: ≤ 2,500	Heating	Experimental and numerical	Stainless steel tube with inside diameter of 2.0 mm
Jiang et al. [62]	86	25 and 30	60.3–546	Inlet Reynolds numbers 4.0×10^3–1.06×10^4 Re: ≥ 4,000	Heating	Experimental and numerical	Stainless steel tube with inside and outside diameters of 0.27 mm and 1.59 mm
Jiang et al. [63]	77–97	30–45	22–89	m: 0.5–2.4 kg/h	Heating	Experimental and numerical	Sintered porous tubes with particle diameters of 0.1–0.12 mm and 0.2–0.28 mm
Kim et al. [64]	81.2		30–50	G: 400–1,200 kg/(m^2 s)	Cooling		Tubes of 4.4 mm and 9.0 mm IDs, and a concentric annular passage (ϕ8 mm × ϕ10 mm × L1800 mm)

Bae and Kim. [65]	77.5–88.5	5–27	Up to 150	G: 400–1,200 kg/(m^2 s)	Cooling	Experimental	Tubes of 4.4 mm and 9.0 mm IDs, and a concentric annular passage (ϕ8 mm × ϕ10 mm × L1800 mm)
Cho et al. [66]	81.2	27.2	50–130	G: 1,200 kg/(m^2 s)	Cooling	Numerical	Stainless steel tube of 4.4 mm ID and an 8/10 mm annular channel
Bruch et al. [67]	74–120	Bulk 15–70		m: 5–60 kg/h G: 50–590 kg/(m^2 s) Re: 3.6×10^3–1.8×10^6	Cooling	Experimental	Copper tubes with an inner diameter of 6 mm
Li et al. [68]	78–95	25–40	6.4–520	m: 1.6–3.68 kg/h Re: 3.8×10^3–2×10^4	Heating	Experimental	Stainless steel tube with inside diameter of 2.0 mm
Bae et al. [69]	77.5–81.2	5–37	30–170	G: 285–1,200 kg/(m^2 s)	Heating	Experimental	Stainless steel circular tube with an inner diameter of 6.32 mm
Kim and Kim [70]	74.6–102.6	Bulk 29–115	38–234	G: 208–874 kg/(m^2 s)	Heating		Stainless steel tubes with inner and out diameters of 4.5 mm and 6.3 mm
Zahlan et al. [71]	59.1–86.7	7.1–13.8	2.9–436	G: 193–2,041 kg/(m^2 s)	Heating	Experimental	Stainless steel tubes with inner diameters of 8 mm and 22 mm
Xu et al. [72]	76.5	22.5–24.5	9.6–79.6	Re: 3.2×10^3–5.4×10^3	Heating	Experimental	Stainless steel tubes with inner and outer diameters of 0.953 mm and 2.1 mm, one straight and one serpentine, and the serpentine section including 3.5 serpentine

							units with each serpentine unit including four bend units with bend diameters of 8.01 mm
Pidaparti et al. [36]	75–102	20–55	13.5–62.5	*G*: 150–350 kg/(m^2 s)	Heating	Experimental	Stainless steel tube with inner and outer diameters of 10.9 mm and 12.7 mm
Zhang et al. [41, 73]	75–90	15	10–70	*G*: 80–600 kg/(m^2 s)	Heating	Experimental	Stainless steel tube with an inner diameter of 4 mm and wall thickness of 2 mm.
Zhu et al. [74]	75–211	10-120	74–413	*G*: 488–1600 kg/(m^2 s)	Heating	Experimental	Stainless steel tube with an inner diameter of 10 mm and wall thickness of 2 mm.
Wang et al. [75]	76.6–90	30.8–37	21.7–353.7	*G*: 672-4810 kg/(m^2 s)	Heating	Experimental	Stainless steel tubes with a fixed outer diameter of 1.6 mm and three inner diameters of 1.0 mm, 0.75 mm and 0. 5 mm.

Table 4 Investigated factors influencing heat transfer inside vertical channels.

Reference	Mass flux	Heat flux	Bulk temperature	Pressure	Tube diameter	Flow direction	Buoyancy
Bourke et al. [52]	√	√	√	√			√
Liao and Zhao [22]	√	√	√	√	√		√
Jiang et al. [53]	√	√	√		√		√
He et al. [54]	√	√	√	√			√
He et al. [55]	√	√	√	√			√
Jiang et al. [56]	√	√	√	√	√	√	√
Kim et al. [57]	√	√	√		√		√
Kim et al. [58]	√	√	√	√			
Kim et al. [59]	√	√	√	√		√	√

Jiang et al. [60]	√	√	√					√
Jiang et al. [61]	√	√	√	√				√
Jiang et al. [62]	√	√	√				√	√
Jiang et al. [63]	√	√	√	√			√	√
Kim et al. [64]	√	√	√					√
Bae and Kim. [65]	√	√	√	√	√			√
Cho et al. [66]	√	√	√					
Bruch et al. [67]	√	√	√	√			√	√
Li et al. [68]	√	√	√	√			√	√
Bae et al. [69]	√	√	√	√	√		√	√
Kim and Kim [70]	√	√	√	√				√

Zahlan et al. [71]	√	√	√	√	√		√
Xu et al. [72]	√	√	√			√	√
Pidaparti et al. [36]	√	√	√	√		√	√
Zhang et al. [41, 73]	√	√	√	√		√	√
Zhu et al. [74]	√	√	√	√			√
Wang et al. [75]	√	√	√	√	√	√	√

Table 5 Summary of heat transfer of CO_2 at supercritical pressure flowing inside helical coils.

Reference	**Pressure** ***P*** **(bar)**	**Inlet temperature** ***T*** **(°C)**	**Heat flux** ***q*** **(kW/m^2)**	**Flow rate**	**Working condition**	**Method**	**Flow geometry**
Zhang et al. [77]	80.2–100.5	15	0.4–50	*G*: 0–650 kg/(m^2 s)	Heating	Experimental	Stainless steel with an inner diameter of 9.05 mm, outer diameter of 12.05 mm, and length of 5,500.26 mm, comprising six coil turns with coil diameter of 283.05 mm and pitch of 32.05 mm
Wang et al. [78]	80	15	10–50	*G*: 97.8–300 kg/(m^2 s)	Heating	Numerical	Helically coiled tube with tube radius of 141.5 mm, coil radius of 9 mm, coil pitch of 32 mm and length of 5,500 mm
Wang et al. [79]	80–90		4.2–24.3	*G*: 159–318.2 kg/(m^2 s)	Cooling	Experimental	Copper coiled tube 560 mm long, with an inner diameter of 4 mm, an outer diameter of 6 mm, a coil pitch 2πb of 34 mm and a coil radius of 36 mm
Liu et al. [80]	75–90	Bulk 20-55	9–39.9	*m*: 1–4 g/s	Cooling	Experimental and numerical	Coiled tube with inner diameter of 4 and 6 mm, a coil pitch of 34 mm and coil diameter of 36-140 mm.
Zhang et al. [41]	75–90	15	10–62	*G*: 80–600 kg/(m^2 s)	Heating	Experimental and numerical	Stainless steel with an inner diameter of 4 mm and wall thickness of 1 mm, coil diameter of 160 mm and pitch of 20 mm.
Liu et al. [81]	75–90	Bulk 20-55	17.8–24.5	*G*: 120 kg/(m^2 s)	Cooling	Experimental and numerical	Coiled tube with inner and outer diameter of 8 and 9 mm, a coil pitch of 36 mm and coil diameter of 300 mm.

Table 6 Investigated factors influencing heat transfer inside helical coils.

Reference	Mass flux	Heat flux	Bulk temperature	Pressure	Tube diameter	Flow direction	Buoyancy
Zhang et al. [77]	√	√	√	√			√
Wang et al. [78]	√	√	√				√
Wang et al. [79]	√	√	√	√			√
Liu et al. [80]	√	√	√	√			√
Zhang et al. [41]	√	√	√	√		√	√
Liu et al. [81]	√	√	√	√		√	√

Table 7 Summary of modification of Dittus–Boelter correlation for CO_2 at supercritical pressure flowing inside channels.

Author(s)	**Correlations**	**Remarks**
Bringer and Smith [85]	$Nu_{\mathrm{b}} = 0.0375 Re_{\mathrm{b}}^{0.77} Pr_{\mathrm{w}}^{0.55}$ Reference temperature T is defined as $T = T_{\mathrm{b}}$, if $(T_{\mathrm{pc}} - T_{\mathrm{b}}) / (T_{\mathrm{w}} - T_{\mathrm{b}}) < 0$ $T = T_{\mathrm{pc}}$, if $0 \le (T_{\mathrm{pc}} - T_{\mathrm{b}}) / (T_{\mathrm{w}} - T_{\mathrm{b}}) \le 1$ $T = T_{\mathrm{b}}$, if $(T_{\mathrm{pc}} - T_{\mathrm{b}}) / (T_{\mathrm{w}} - T_{\mathrm{b}}) > 1$	Based on the experimental data presented in their paper for CO_2 heated in a horizontal tube Reynolds number 30,000 to 300,000 Heat transfer rate 78,000–282,000 Btu/hr ft^2 Temperature 70 to 120 °F.
Liao and Zhao [17, 22]	In horizontal flow, cooled at a constant temperature $Nu_{\mathrm{b}} = 0.128 Re_{\mathrm{w}}^{0.8} Pr_{\mathrm{w}}^{0.3} \left(\frac{Gr}{Re_{\mathrm{b}}^2}\right)^{0.205} \left(\frac{\rho_{\mathrm{b}}}{\rho_{\mathrm{w}}}\right)^{0.437} \left(\frac{\bar{c}_{\mathrm{p}}}{c_{\mathrm{pw}}}\right)^{0.411}$ In horizontal flow, heated at a constant temperature $Nu_{\mathrm{b}} = 0.124 Re_{\mathrm{b}}^{0.82} Pr_{\mathrm{b}}^{0.4} \left(\frac{Gr}{Re_{\mathrm{b}}^2}\right)^{0.203} \left(\frac{\rho_{\mathrm{w}}}{\rho_{\mathrm{b}}}\right)^{0.842} \left(\frac{\bar{c}_{\mathrm{p}}}{c_{\mathrm{pb}}}\right)^{0.384}$ In upward flow, heated at a constant temperature $Nu_{\mathrm{b}} = 0.354 Re_{\mathrm{b}}^{0.8} Pr_{\mathrm{b}}^{0.4} \left(\frac{Gr_{\mathrm{m}}}{Re_{\mathrm{b}}^{2.7}}\right)^{0.157} \left(\frac{\rho_{\mathrm{w}}}{\rho_{\mathrm{b}}}\right)^{1.297} \left(\frac{\bar{c}_{\mathrm{p}}}{c_{\mathrm{pb}}}\right)^{0.296}$ In downward flow, heated at a constant temperature $Nu_{\mathrm{b}} = 0.643 Re_{\mathrm{b}}^{0.8} Pr_{\mathrm{b}}^{0.4} \left(\frac{Gr_{\mathrm{m}}}{Re_{\mathrm{b}}^{2.7}}\right)^{0.186} \left(\frac{\rho_{\mathrm{w}}}{\rho_{\mathrm{b}}}\right)^{2.154} \left(\frac{\bar{c}_{\mathrm{p}}}{c_{\mathrm{pb}}}\right)^{0.751}$	Based on the experimental data presented in their paper Long tubes of $0.7 \le d \le 2.16$ mm in the range of $74 \le p \le 120$ bar, $20 \le T_{\mathrm{b}} \le 110$ °C, $2 \le \lvert T_{\mathrm{w}} - T_{\mathrm{b}} \rvert \le 30$ °C, $0.02 \le \dot{m} \le 0.2$ kg/min, $10^{-5} \le Gr/Re_{\mathrm{b}}^2 \le 10^{-2}$ for horizontal flow, $2\times10^{-9} \le Gr/Re_{\mathrm{b}}^{2.7} \le 10^{-5}$ for upward and downward flows.
Yoon et al. [24]	$Nu_{\mathrm{b}} = 0.14 Re_{\mathrm{b}}^{0.69} Pr_{\mathrm{b}}^{0.66}$, if $T_{\mathrm{b}} > T_{\mathrm{pc}}$ $Nu_{\mathrm{b}} = 0.013 Re_{\mathrm{b}} Pr_{\mathrm{b}}^{-0.05} \left(\frac{\rho_{\mathrm{pc}}}{\rho_{\mathrm{b}}}\right)^{1.6}$, if $T_{\mathrm{b}} \le T_{\mathrm{pc}}$	Based on the experimental data presented in their paper for CO_2 cooled in a horizontal tube.

Huai et al. [27]	$Nu_b = 2.2186 \times 10^{-2} Re_b^{0.8} Pr_b^{0.3} (\frac{\rho_b}{\rho_w})^{-1.4652} (\frac{\bar{c_p}}{c_{pw}})^{0.0832}$	Based on the experimental data presented in their paper for CO_2 heated in multi-port horizontal tubes $74 < p < 85$ bar, $74 < T_r < 53$ ˚C, $113.7 < G < 418.6$ kg/(m^2 s), and $0.8 < q < 9$ kW/m^2.
Son et al. [28]	$Nu_b = Re_b^{0.55} Pr_b^{0.23} (\frac{c_{pb}}{c_{pw}})^{0.15}$, if $T_b > T_{pc}$ $Nu_b = Re_b^{0.35} Pr_b^{1.9} (\frac{\rho_b}{\rho_w})^{-1.6} (\frac{c_{pb}}{c_{pw}})^{-3.4}$, if $T_b \leq T_{pc}$	Based on the experimental data presented in their paper for CO_2 cooled in a horizontal tube.
Kim et al. [57]	$Nu_b = Nu_0 (\frac{\xi_M}{\xi_F}) (\frac{\bar{c_p}}{c_{pb}})^{0.6} (\frac{\rho_w}{\rho_b})^n$	Based on the experimental data presented in their paper for CO_2 heated in vertical tubes with circular, triangular, and square cross-sections.
Oh and Son [31]	$Nu_b = 0.023 Re_b^{0.7} Pr_b^{2.5} (\frac{c_{pb}}{c_{pw}})^{-3.5}$ for $T_b > T_{pc}$ $Nu_b = 0.023 Re_b^{0.6} Pr_b^{3.2} (\frac{\rho_b}{\rho_w})^{3.7} (\frac{c_{pb}}{c_{pw}})^{-4.6}$ for $T_b \leq T_{pc}$	After review of the existing literature and data, horizontal macro tube under cooling conditions.
Kim and Kim [70]	$Nu_b = 0.0226 Re_b^{1.174} Pr_b^{1.057} (\frac{\rho_w}{\rho_b})^{0.571} (\frac{\bar{c_p}}{c_{pb}})^{1.032} A^{0.489} B^{0.0021}$	Based on the experimental data presented in their paper for CO_2 heated in a vertical tube
Lee et al. [35]	$Nu_b = Re_b^{0.55} Pr_b^{0.3} (\frac{\rho_b}{\rho_w})^{-0.4}$ for $T_b > T_{pc}$ $Nu_b = Re_b^{0.56} Pr_b^{0.27} (\frac{c_{pb}}{c_{pw}})^{0.2}$ for $T_b > T_{pc}$ $Nu_b = Re_b^{0.47} Pr_b^{0.98} (\frac{\rho_b}{\rho_w})^{0.3}$ for $T_b \leq T_{pc}$ $Nu_b = Re_b^{0.35} Pr_b^{2.0} (\frac{c_{pb}}{c_{pw}})^{-3}$ for $T_b \leq T_{pc}$ $Nu_b = Re_b^{0.37} Pr_b^{2.1} (\frac{\rho_b}{\rho_w})^{-1.7} (\frac{c_{pb}}{c_{pw}})^{-3.6}$ for $T_b \leq T_{pc}$	Based on the experimental data presented in their paper for CO_2 cooled in a horizontal smooth tube and a micro-fin tube.

Zhang et al. [77]	For the low-enthalpy region below the pseudo-critical temperature $Nu_{\mathrm{b}} = 0.32Re_{\mathrm{b}}^{0.55}Pr_{\mathrm{b}}^{0.35}(\frac{\rho_{\mathrm{w}}}{\rho_{\mathrm{b}}})^{0.11}(\frac{\overline{c_{\mathrm{p}}}}{c_{\mathrm{pb}}})^{0.37}$ for $T_{\mathrm{b}} \le T_{\mathrm{pc}}$ For the high-enthalpy region below the pseudo-critical temperature $Nu_{\mathrm{b}} = 0.034Re_{\mathrm{b}}^{0.77}Pr_{\mathrm{b}}^{0.57}(\frac{\rho_{\mathrm{w}}}{\rho_{\mathrm{b}}})^{0.4}(\frac{\overline{c_{\mathrm{p}}}}{c_{\mathrm{pb}}})^{0.84}$ for $T_{\mathrm{b}} > T_{\mathrm{pc}}$	Based on the experimental data presented in their paper for CO_2 heated in a vertical helically coiled tube under constant-heat-flux conditions.
Guo et al. [44]	$Nu_{\mathrm{b}} = 0.114Re_{\mathrm{b}}^{0.589}Pr_{\mathrm{b}}^{0.465}(\frac{Gr}{Re_{\mathrm{b}}^2})^{-0.125}(\frac{\rho_{\mathrm{w}}}{\rho_{\mathrm{b}}})^{0.240}(\frac{\overline{c_{\mathrm{p}}}}{c_{\mathrm{pb}}})^{0.096}$	Based on the experimental data presented in their paper for CO_2 heated in mini tubes $76 < p < 84$ bar, $400 < G < 700$ kg/(m^2 s), $100 < q < 200$ kW/m^2, and $250 < q/G < 500$ J/kg.
Wahl et al. [45]	$Nu_{\mathrm{w}} = 0.0495Re_{\mathrm{w}}^{0.771}Pr_{w}^{0.455}(\frac{\rho_{\mathrm{b}}}{\rho_{\mathrm{w}}})^{1.450}(\frac{\overline{c_{\mathrm{p}}}}{c_{\mathrm{pb}}})^{-0.026}(\frac{\lambda_{\mathrm{b}}}{\lambda_{\mathrm{w}}})^{1.604}(\frac{\eta_{\mathrm{b}}}{\eta_{\mathrm{w}}})^{-2.623}$ for $T_{\mathrm{w}} \ge T_{\mathrm{pc}}$ $Nu_{\mathrm{w}} = 0.0052Re_{\mathrm{w}}^{0.971}Pr_{w}^{0.388}\left(\frac{\rho_{\mathrm{b}}}{\rho_{\mathrm{w}}}\right)^{1.279}(\frac{\overline{c_{\mathrm{p}}}}{c_{\mathrm{pb}}})^{0.450}(\frac{\lambda_{\mathrm{b}}}{\lambda_{\mathrm{w}}})^{2.158}(\frac{\eta_{\mathrm{b}}}{\eta_{\mathrm{w}}})^{-2.923}$ for $T_{\mathrm{w}} < T_{\mathrm{pc}}$	Based on the experimental data presented in their paper for CO_2 cooling in a 2 mm tube.
Liu et al. [80]	$Nu_{\mathrm{b}} = 0.02464Re_{\mathrm{b}}^{0.8275}Pr_{\mathrm{b}}^{0.1572}\left(\frac{\rho_{\mathrm{b}}}{\rho_{\mathrm{w}}}\right)^{0.0337}\left(\frac{\overline{c_{\mathrm{p}}}}{c_{\mathrm{pw}}}\right)^{-0.0522}\left(1+\frac{3.54d}{D}\right)^{1.459}$	Based on the experimental data presented in their paper for CO_2 in horizontal helically coiled tube under the cooling condition, coil pitch b = 34 mm, coil diameters D ranging from 36–140 mm and tube diameters d ranging from 2 to 4 mm.

Nu_{o} is Dittus–Boelter correlation, $Gr = \frac{(\rho_{\mathrm{w}}-\rho_{\mathrm{b}})\rho_{\mathrm{b}}gd^3}{\mu_{\mathrm{b}}^2}$, $Gr_{\mathrm{m}} = \frac{(\rho_{\mathrm{b}}-\rho_{\mathrm{m}})\rho_{\mathrm{b}}gd^3}{\mu_{\mathrm{b}}^2}$, $\rho_{\mathrm{m}} = \frac{1}{T_{\mathrm{w}}-T_{\mathrm{b}}}\int_{T_{\mathrm{b}}}^{T_{\mathrm{w}}}\rho\, dT$, $\overline{c_{\mathrm{p}}} = (h_{\mathrm{b}}-h_{\mathrm{w}})/(T_{\mathrm{b}}-T_{\mathrm{w}})$, $\xi_{\mathrm{M}} = \frac{8\tau_{\mathrm{w}}}{\rho_{\mathrm{b}}u_{\mathrm{b}}^2}$, $\tau_{\mathrm{w}} = \rho_{\mathrm{w}}u_{\tau}^2$, $\frac{u_{\mathrm{b}}}{u_{\tau}} = \frac{1}{0.41}\ln(\frac{yu_{\tau}}{\upsilon_{\mathrm{b}}}) + 5.0$, $\xi_{\mathrm{F}} = \frac{1}{(1.8\log(Re_{\mathrm{b}})-1.5)^2}$,

$A = \frac{q^+}{Re_{\mathrm{b}}^{0.625}}(\frac{\mu_{\mathrm{w}}}{\mu_{\mathrm{b}}})(\frac{\rho_{\mathrm{b}}}{\rho_{\mathrm{w}}})^{0.5}$, $B = \frac{Gr_{\mathrm{q}}}{Re_{\mathrm{b}}^{3.425}Pr^{0.8}}(\frac{\mu_{\mathrm{w}}}{\mu_{\mathrm{b}}})(\frac{\rho_{\mathrm{b}}}{\rho_{\mathrm{w}}})^{0.5}$, $Gr_{\mathrm{q}} = \frac{g\beta d^4q_{\mathrm{w}}}{k\upsilon^2}$, $q^+ = \frac{\beta q_{\mathrm{w}}}{Gc_{\mathrm{p}}}$, $n = 0.955 - 0.0087\left(\frac{q}{G}\right) + 1.3\times10^{-5}\left(\frac{q}{G}\right)^2$.

Table 8 Summary of modification of Petukhov and Kirillov correlation for CO_2 at supercritical pressure flowing inside channels.

Author(s)	**Correlations**	**Remarks**
Krasnoshchekov and Protopopov [86]	$Nu_b = Nu_0(\frac{\mu_b}{\mu_w})^{0.11}(\frac{k_b}{k_w})^{-0.33}(\frac{\overline{c_p}}{c_{pb}})^{0.35}$	Based on the experimental data presented in their paper for CO_2 heated in vertical and horizontal tubes $2\times10^4 < Re_b < 8.6\times10^5$, $0.85 < \overline{Pr_b} < 65$, $0.90 < \frac{\mu_b}{\mu_w} < 3.6$, $1 < \frac{k_b}{k_w} < 6$ and $0.07 < \frac{\overline{c_p}}{c_{pb}} < 4.5$.
Krasnoshchekov [87]	$Nu_b = Nu_0(\frac{\rho_w}{\rho_b})^{0.3}(\frac{\overline{c_p}}{c_{pb}})^{n}$ $n = 0.4$, for $(T_w / T_{pc}) \leq 1$ or $(T_b / T_{pc}) \geq 1.2$ $n = n_1 = 0.22 + 0.18\ (T_w / T_{pc})$, for $1 \leq (T_w / T_{pc}) \leq 2.5$ $n = n_1 + (5n_1 - 2)(1 - (T_b / T_{pc}))$, for $1 \leq (T_b / T_{pc}) \leq 1.2$ where T_b, T_{pc}, and T_w are in Kelvin	Based on the experimental data presented in their paper for CO_2 heated in vertical and horizontal tubes $8\times10^4 < Re_b < 5\times10^5$, $0.85 < \overline{Pr_b} < 65$, $0.09 < \frac{\rho_w}{\rho_b} < 10$, $0.02 < \frac{\overline{c_p}}{c_{pb}} < 4$, $0.9 \leq (T_w / T_{pc}) \leq 2.5$, $4.6\times10^4 < q < 2.6\times10^6$ (q is in W/m^2).

Nu_o is Petukhov and Kirillov correlation.

Table 9 Summary of modification of Gnielinski correlation for CO_2 at supercritical pressure flowing inside channels.

Author(s)	**Correlations**	**Remarks**
Pitla et al. [23]	$Nu = \left(\frac{Nu_{\mathrm{w}} + Nu_{\mathrm{b}}}{2}\right)\frac{k_{\mathrm{w}}}{k_{\mathrm{b}}}$ Nu_{w} and Nu_{b} are respectively calculated by Gnielinski correlation.	Based on the numerical predictions presented in their paper for CO_2 cooled in a horizontal tube.
Dang and Hihara [25]	$Nu = \frac{(\xi/8)(Re_{\mathrm{b}} - 1{,}000)Pr}{12.7\sqrt{\xi/8}(Pr^{2/3} - 1) + 1.07}$ $Pr = c_{\mathrm{pb}}\mu_{\mathrm{b}}/k_{\mathrm{b}}$, for $c_{\mathrm{pb}} \geq \bar{c_{\mathrm{p}}}$ $Pr = \bar{c_{\mathrm{p}}}\mu_{\mathrm{b}}/k_{\mathrm{b}}$, for $c_{\mathrm{pb}} < \bar{c_{\mathrm{p}}}$ and $\mu_{\mathrm{b}}/k_{\mathrm{b}} \geq \mu_{\mathrm{f}}/k_{\mathrm{f}}$ $Pr = \bar{c_{\mathrm{p}}}\mu_{\mathrm{b}}/k_{\mathrm{b}}$, for $c_{\mathrm{pb}} < \bar{c_{\mathrm{p}}}$ and $\mu_{\mathrm{b}}/k_{\mathrm{b}} < \mu_{\mathrm{f}}/k_{\mathrm{f}}$ where subscript b represents the bulk temperature, and f the film temperature.	Based on the experimental data presented in their paper for CO_2 cooled in a horizontal tube.

$\bar{c_{\mathrm{p}}} = (h_{\mathrm{b}} - h_{\mathrm{w}})/(T_{\mathrm{b}} - T_{\mathrm{w}})$, $\xi = \frac{1}{(1.82\log_{10}Re_{\mathrm{b}} - 1.64)^2}$.

Table 10 Summary of modification of Jackson correlation for CO_2 at supercritical pressure flowing inside channels.

Author(s)	**Correlations**	**Remarks**
Kim et al. [59]	$Nu_b = Nu_0 f(B)$	Based on the experimental data presented in their paper for
	$f(B) = (0.8 + 6.0 \times 10^6 B)^{-0.8}$, for $B \leq 7.0\times10^{-8}$	CO_2 heated in a concentric annular passage.
	$f(B) = 0.261 + 3.068 \times B^{0.1}$, for $7.0\times10^{-8} < B \leq 7.0\times10^{-7}$	
	$f(B) = 1.47 - 6.7 \times 10^5 B$, for $7.0\times10^{-7} < B \leq 1.0\times10^{-6}$	
	$f(B) = 0.8$, for $1.0\times10^{-6} < B \leq 1.0\times10^{-5}$	
	$f(B) = 0.1423 \times B^{-0.15}$, for $1.0\times10^{-5} < B$	
Bae and Kim. [65]	$Nu_b = Nu_0 f(B)$	Based on the experimental data presented in their paper for
	$f(B) = (1 + 1.0 \times 10^8 B)^{-0.032}$, for $5.0\times10^{-8} < B < 7.0\times10^{-7}$	CO_2 cooled in a concentric annular passage.
	$f(B) = 0.0185 \times B^{-0.43465}$, for $7.0\times10^{-7} < B < 1.0\times10^{-6}$	
	$f(B) = 0.75$, for $1.0\times10^{-6} < B < 1.0\times10^{-5}$	
	$f(B) = 0.0119 \times B^{-0.36}$, for $1.0\times10^{-5} < B < 3.0\times10^{-5}$	
	$f(B) = 32.4 \times B^{0.4}$, for $3.0\times10^{-5} < B < 1.0\times10^{-4}$	
Bruch et al. [67]	$Nu_b = Nu_0 f$	Based on the experimental data presented in their paper for
	In turbulent aiding mixed convection,	CO_2 cooled in a vertical tube.
	$f = 1 - 75(\frac{Gr}{Re_b^{2.7}})^{0.46}$ for $Gr/Re_b^{2.7} < 4.2 \times 10^{-5}$	
	$f = 13.5(\frac{Gr}{Re_b^{2.7}})^{0.4}$ for $\frac{Gr}{Re_b^{2.7}} > 4.2 \times 10^{-5}$	
	In turbulent opposing mixed convection,	
	$f = (1.542 - 3{,}243(\frac{Gr}{Re_b^{2.7}})^{0.91})^{1/3}$	

Li et al. [68]	$Nu_{\mathrm{b}} = Nu_0 f \varepsilon$ $f = (1 + (Bo^*)^{0.1}(\frac{\rho_{\mathrm{w}}}{\rho_{\mathrm{b}}})^{0.5}(\frac{\overline{c_{\mathrm{p}}}}{c_{\mathrm{pb}}})^{-0.3} f^{-2})^{0.46}$ for downward flow $f = (\left\|1 - (Bo^*)^{0.1}(\frac{\rho_{\mathrm{w}}}{\rho_{\mathrm{b}}})^{0.35}(\frac{\overline{c_{\mathrm{p}}}}{c_{\mathrm{pb}}})^{-0.009} f^{-2}\right\|)^{0.46}$ for upward flow	Based on the experimental data presented in their paper for CO_2 heated in a vertical tube.
Bae et al. [69]	$Nu_{\mathrm{b}} = Nu_0 f(B)$ For normal heat transfer of upward flow $f(B) = (1 + 3 \times 10^5 B)^{0.35}$, for $B < 2\times10^{-6}$ $f(B) = 0.48 \times B^{-0.07}$, for $B > 2\times10^{-6}$ For deteriorated heat transfer of upward flow $f(B) = 1$, for $B < 2\times10^{-7}$ $f(B) = 0.043 \times B^{-0.2}$, for $2\times10^{-7} < B < 6\times10^{-6}$ $f(B) = 1{,}120 \times B^{0.64}$, for $6\times10^{-6} < B < 1.5\times10^{-5}$ $f(B) = 3.6 \times 10^{-8} B^{-1.53}$, for $1.5\times10^{-5} < B < 4\times10^{-5}$ $f(B) = 200 \times B^{0.68}$, for $4\times10^{-5} < B < 2\times10^{-4}$ For downward flow $f(B) = 1$, for $B < 10^{-7}$ $f(B) = 0.153 \times B^{-0.117}$, for $10^{-7} < B < 8 \times 10^{-6}$ $f(B) = 15.8 \times B^{0.28}$, for $8 \times 10^{-6} < B < 5 \times 10^{-5}$	Based on the experimental data presented in their paper for CO_2 heated in a vertical tube.
Li et al. [34]	$Nu_{\mathrm{b}} = 0.023 Re_{\mathrm{b}}^{0.8} Pr_{\mathrm{b}}^{0.4}(\frac{\rho_{\mathrm{w}}}{\rho_{\mathrm{b}}})^{0.3}(\frac{\overline{c_{\mathrm{p}}}}{c_{\mathrm{pb}}})^{n}$	Based on the experimental data presented in their paper for CO_2 in horizontal tube under both heating and cooling.

	$\overline{c_p} = (h_b - h_w)/(T_b - T_w)$
	n = 0.4, for (T_b / T_{pc}) < (T_w / T_{pc}) ≤ 1 or (T_w / T_{pc}) ≥ (T_b / T_{pc}) ≥ 1.2
	n = 0.4 + 0.2 ((T_w / T_{pc}) – 1), for T_b / T_{pc}) ≤ 1 ≤ (T_w / T_{pc})
	n = 0.4 + 0.2 ((T_w / T_{pc}) – 1)(1 – 5(T_b / T_{pc}) – 1), for 1 ≤ (T_b / T_{pc}) ≤ 1.2 and (T_b / T_{pc}) <
	(T_w / T_{pc})
	where T_b, T_{pc}, and T_w are in Kelvin

Nu_o is Jackson correlation, $B = \frac{\overline{Gr}}{Re_b^{2.7}\overline{Pr}^{0.5}}$, $\overline{Gr} = \frac{(\rho_b - \bar{\rho})\rho_b g d^3}{\mu_b^2}$, $\bar{\rho} = \frac{1}{T_w - T_b}\int_{T_b}^{T_w} \rho \, dT$, $\overline{c_p} = (h_b - h_w)/(T_b - T_w)$, $\overline{Pr}_b = \frac{\overline{c_p}}{h_{out} - h_{in}}\int_{h_{in}}^{h_{out}} \frac{\mu(h)}{k(h)} dT$, $Bo^* = \frac{Gr^*}{Re_b^{3.425} Pr^{0.8}}$, $Gr^* = \frac{g\beta d^4 q_w}{k\upsilon^2}$, $\varepsilon = 1 + 2.35 Re_b^{-0.15} Pr_b^{-0.4} (x/d)^{0.6} \exp(-0.39 Re_b^{-0.1} (x/d))$.

Fig. 1 Thermophysical properties of CO_2 at different pressures and temperatures (REFPROP V9.1): (a) Density, (b) Dynamic viscosity, (c) Specific heat and (d) Thermal conductivity.

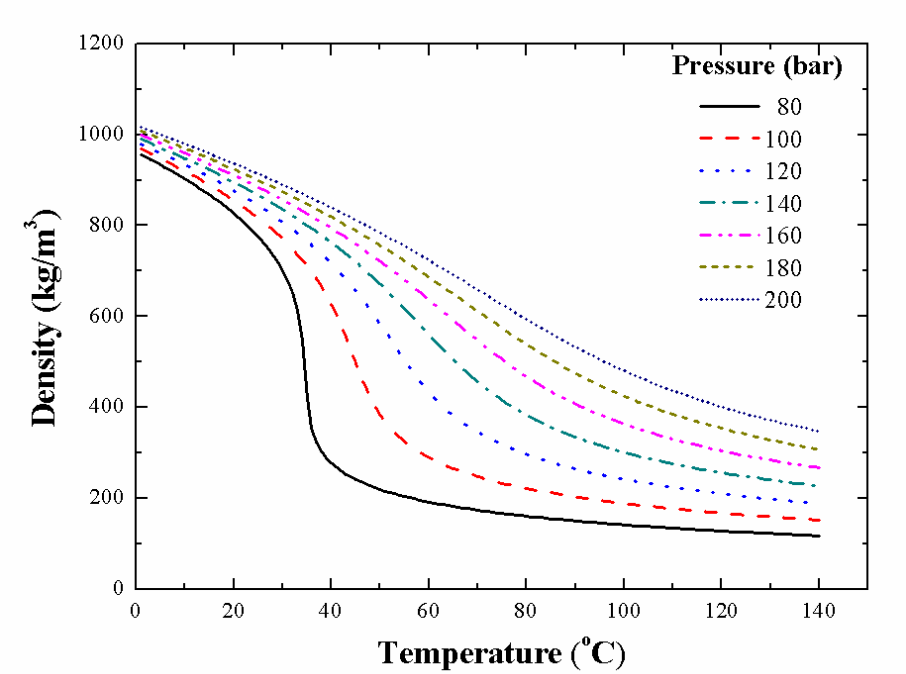

(a)

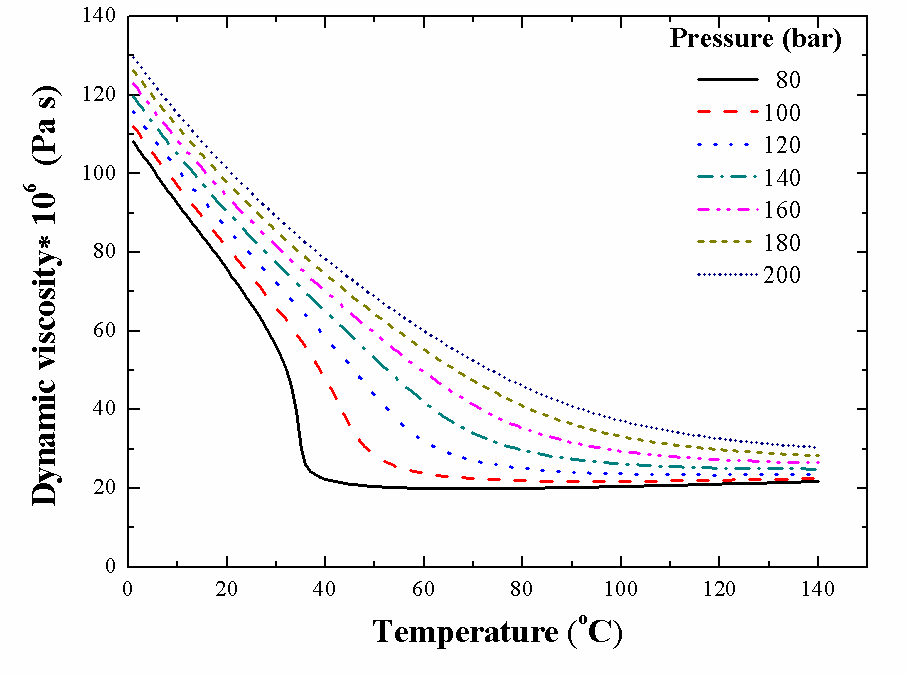

(b)

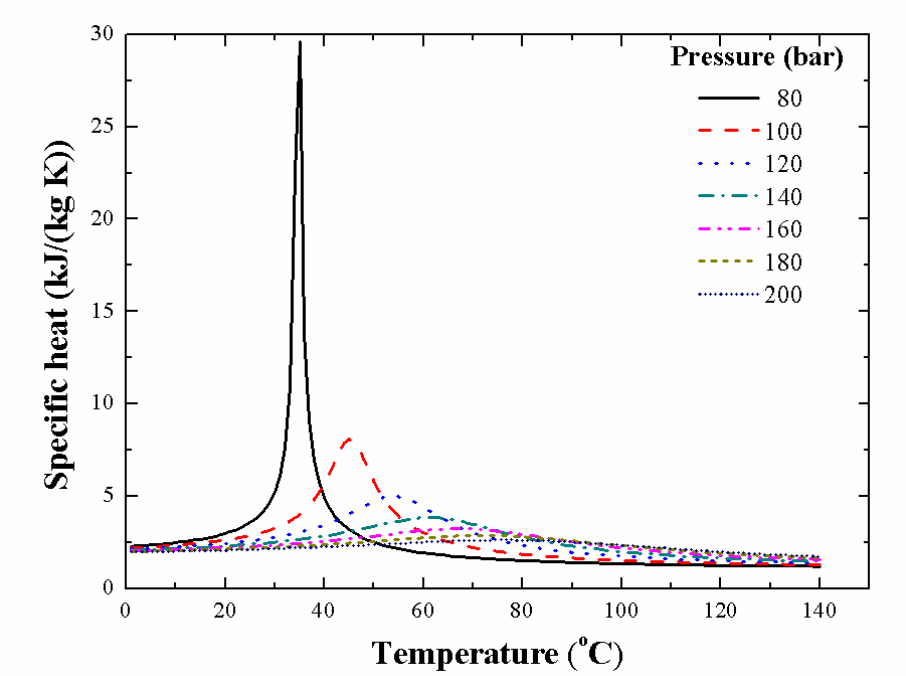
Pressure (bar)
80
100
120
140
160
180
200
Specific heat (kJ/(kg K))
Temperature (°C)
0
5
10
15
20
25
30
0
20
40
60
80
100
120
140

(c)

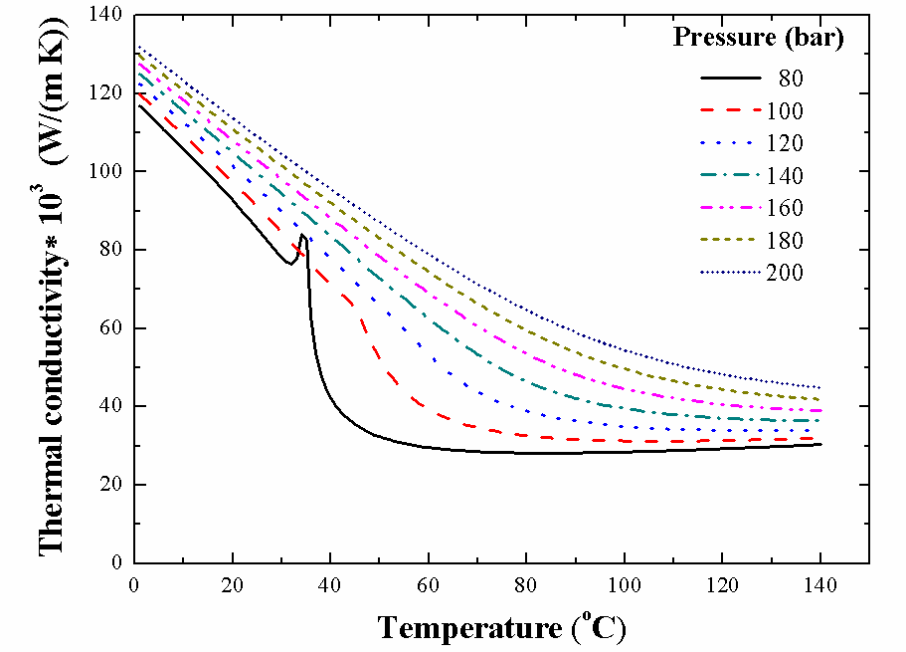
Pressure (bar)
80
100
120
140
160
180
200
Thermal conductivity* 10³ (W/(m K))
Temperature (°C)
0
20
40
60
80
100
120
140
0
20
40
60
80
100
120
140

(d)

Fig. 2 Heat transfer coefficient of CO_2 flowing in horizontal channels [31]: (a) for different inlet pressures and (b) for different mass fluxes.

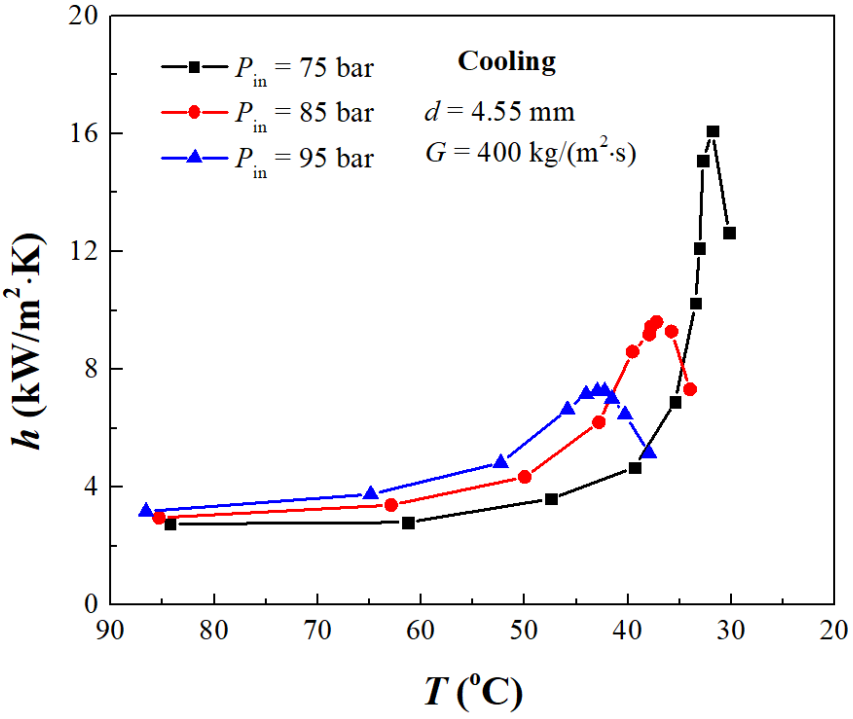

(a)

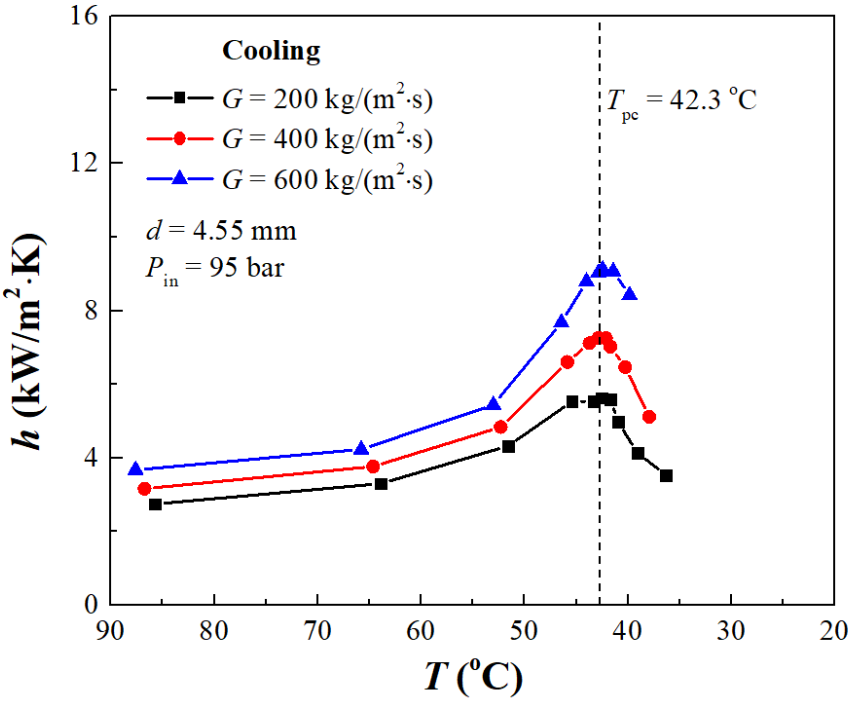

(b)

Fig. 3 Effect of heat flux on heat transfer coefficient of CO_2 flowing in horizontal channels [34]: (a) in heating model and (b) in cooling mode.

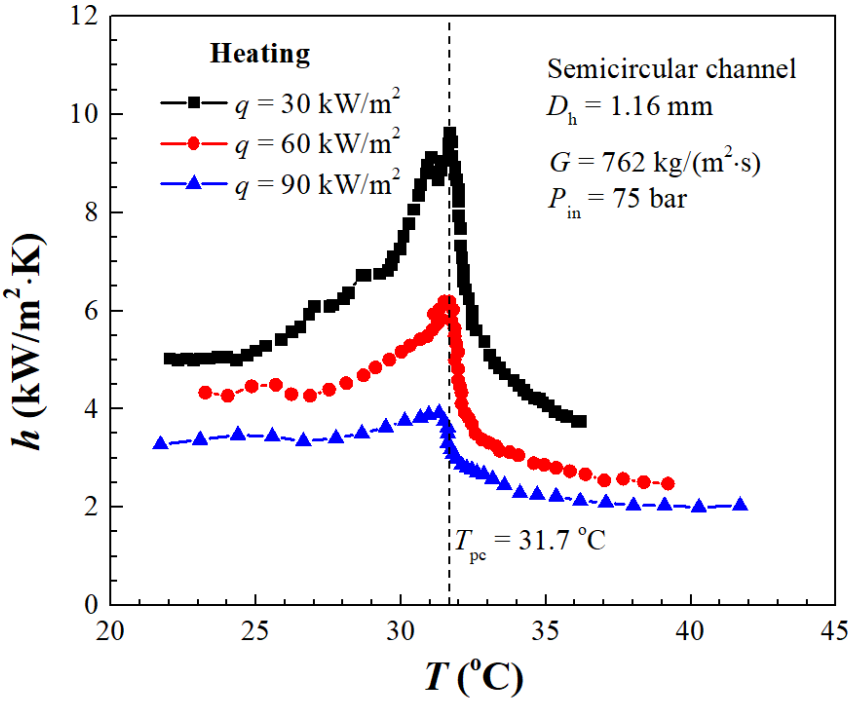

(a)

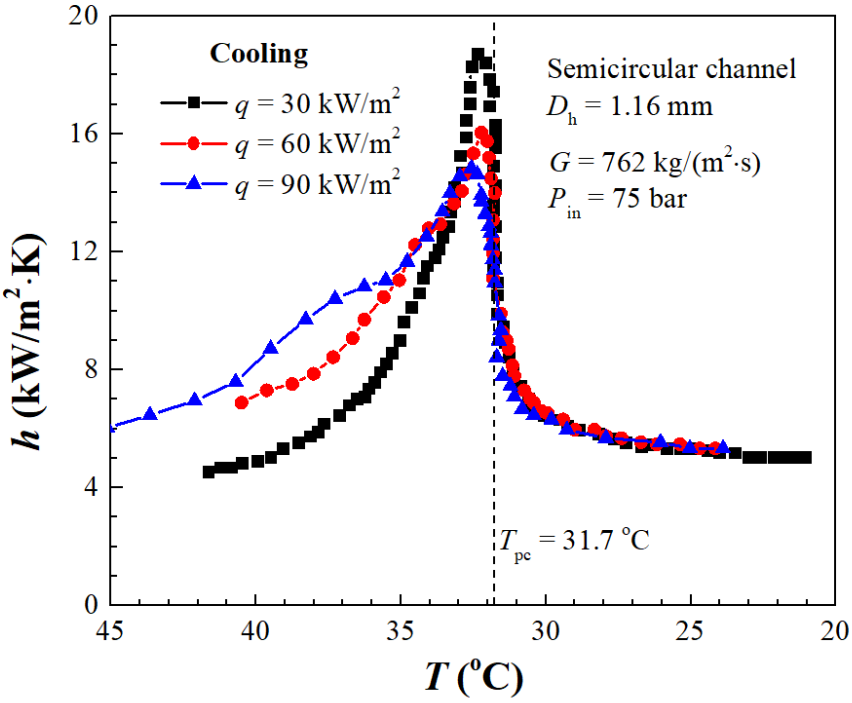

(b)

Fig. 4 Effect of flow direction on heat transfer of CO_2 flowing in macro-tubes [36]: (a) local wall temperature and (b) local heat transfer coefficient.

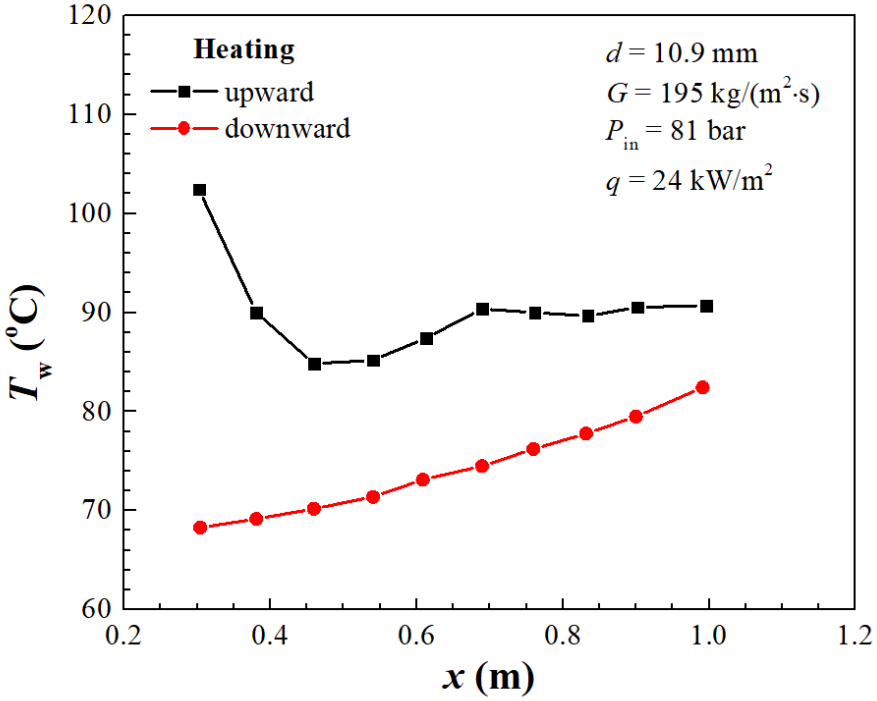

(a)

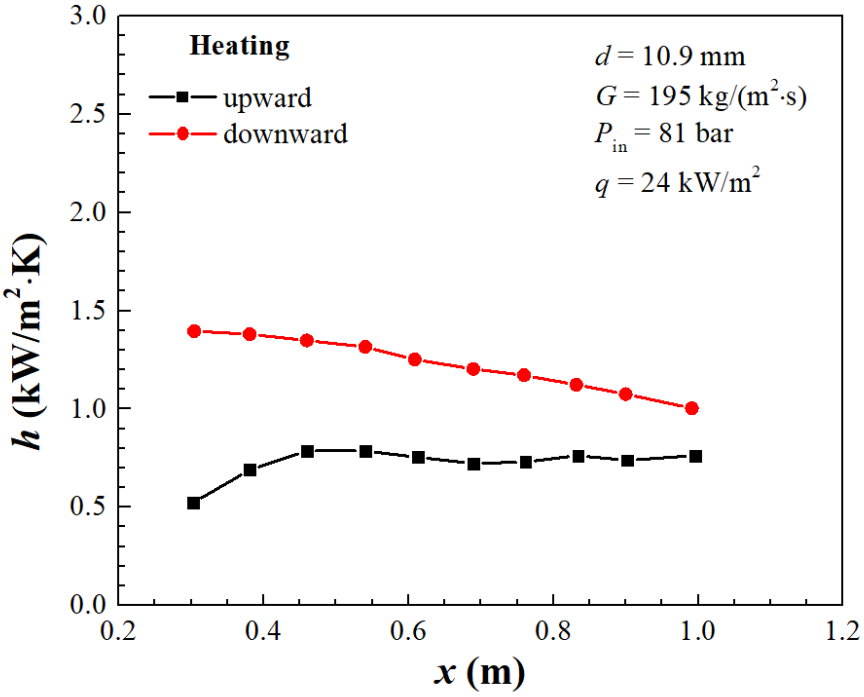

(b)

Fig. 5 Effect of flow direction on heat transfer of CO_2 flowing in microtubes [22]: (a) in 0.7 mm tube and (b) in 1.4 mm tube.

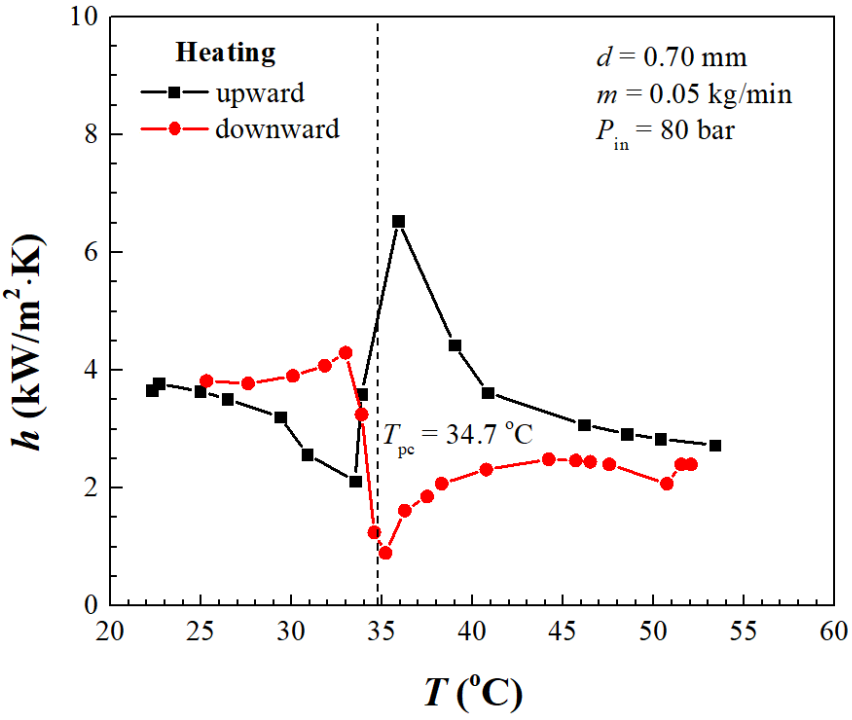

(a)

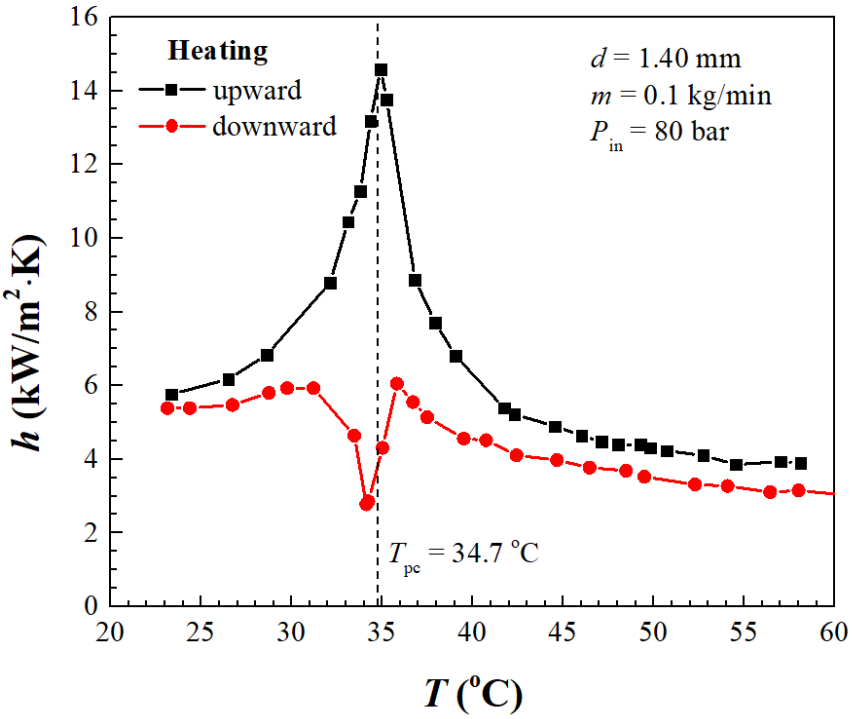

(a)

Fig. 6 Comparison of local heat transfer with empirical correlations [89]: (a) in heating mode and (b) in cooling mode.

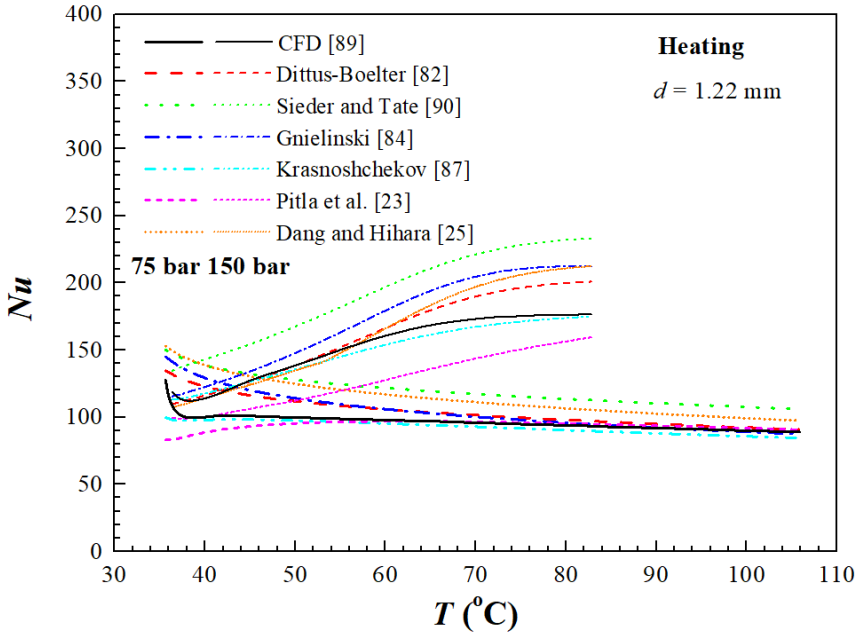

(a)

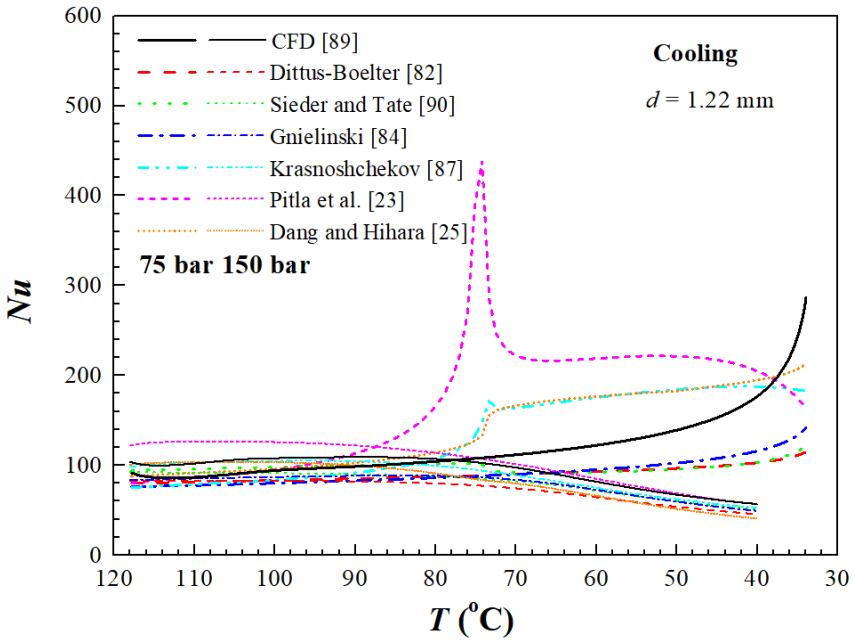

(a)

Fig. 7 Comparison of local friction factor with empirical correlations [89]: (a) in heating mode and (b) in cooling mode.

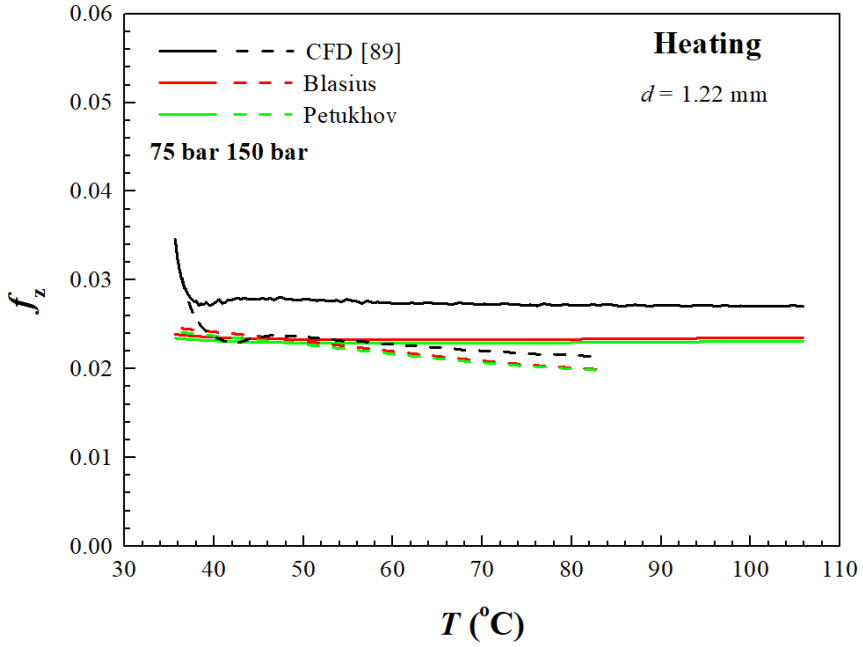

(a)